HHS Public Access

Author manuscript

Nature. Author manuscript; available in PMC 2017 March 15.

Published in final edited form as:

Nature. 2016 September 15; 537(7620): 417–421. doi:10.1038/nature19330.

Defining CD8+ T cells that provide the proliferative burst after PD-1 therapy

Se Jin Im[1], **Masao Hashimoto**[1], **Michael Y. Gerner**[2,3], **Junghwa Lee**[1], **Haydn T. Kissick**[1,4], **Matheus C. Burger**[5], **Qiang Shan**[6], **J. Scott Hale**[1], **Judong Lee**[1], **Tahseen H. Nasti**[1], **Arlene H. Sharpe**[7,8], **Gordon J. Freeman**[9], **Ronald N. Germain**[2], **Helder I. Nakaya**[5], **Hai-Hui Xue**[6,10], and **Rafi Ahmed**[1]

[1]Emory Vaccine Center and Department of Microbiology and Immunology, Emory University School of Medicine, Atlanta, Georgia 30322, USA

[2]Lymphocyte Biology Section, Laboratory of Systems Biology, National Institute of Allergy and Infectious Diseases, National Institutes of Health, Bethesda, Maryland 20892-0421, USA

[3]Department of Immunology, University of Washington School of Medicine, Seattle, Washington 98109, USA

[4]Department of Urology, Emory University School of Medicine, Atlanta, Georgia 30322, USA

[5]School of Pharmaceutical Sciences, University of São Paulo, São Paulo 05508, Brazil

[6]Department of Microbiology, Carver College of Medicine, University of Iowa, Iowa City, Iowa 52242, USA

[7]Department of Microbiology and Immunology, Harvard Medical School, Boston, Massachusetts 02115, USA

[8]Department of Pathology, Brigham and Women's Hospital, Boston, Massachusetts 02115, USA

[9]Department of Medical Oncology, Dana-Farber Cancer Institute, Department of Medicine, Harvard Medical School, Boston, Massachusetts 02115, USA

[10]Interdisciplinary Immunology Graduate Program, Carver College of Medicine, University of Iowa, Iowa City, Iowa 52242, USA

Abstract

Chronic viral infections are characterized by a state of CD8+ T-cell dysfunction that is associated with expression of the programmed cell death 1 (PD-1) inhibitory receptor[1–4]. A better understanding of the mechanisms that regulate CD8+ T cell responses during chronic infection is required to improve immunotherapies that restore function in exhausted CD8+ T cells. Here we

Correspondence and requests for materials should be addressed to R.A. (rahmed@emory.edu).

Author Contributions

R.A, S.J.I., and J.S.H. designed and analysed the experiments. S.J.I., M.H, Jun.L., Jud.L. and T.H.N. performed experiments. S.J.I., H.T.K., M.C.B. and H.I.N. analysed microarray data. M.Y.G. performed immunofluorescence staining and M.Y.G. and R.N.G. analysed data. Q.S., H.H.X., A.H.S., and G.J.F. contributed critical materials. R.A. and S.J.I. wrote the manuscript, with all authors contributing to writing and providing feedback.

R. Ahmed, A.H. Sharpe, and G.J. Freeman declare no additional financial interests. The remaining authors declare no competing financial interests.

identify a population of virus-specific CD8+ T cells that proliferate after blockade of the PD-1 inhibitory pathway in mice chronically infected with lymphocytic choriomeningitis virus (LCMV). These LCMV-specific CD8+ T cells expressed the PD-1 inhibitory receptor but also expressed several costimulatory molecules such as ICOS and CD28. This CD8+ T cell subset was characterized by a unique gene signature that was related to that of CD4+ T follicular helper (T_{FH}) cells, CD8+ T cell memory precursors and haematopoietic stem cell progenitors, but that was distinct from that of CD4+ T_H1 cells and CD8+ terminal effectors. This CD8+ T cell population was found only in lymphoid tissues and resided predominantly in the T cell zones along with naïve CD8+ T cells. These PD-1+ CD8+ T cells resembled stem cells during chronic LCMV infection, undergoing self-renewal and also differentiating into the terminally exhausted CD8+ T cells that were present in both lymphoid and non-lymphoid tissues. The proliferative burst after PD-1 blockade came almost exclusively from this CD8+ T cell subset. Notably, the transcription factor TCF1 had a cell intrinsic and essential role in the generation of this CD8+ T cell subset. These findings provide a better understanding of T cell exhaustion and have implications in the optimization of PD-1-directed immunotherapy in chronic infections and cancer.

Functional exhaustion of antigen-specific CD8+ T cells has been well-documented during persistent infections[1,2] and cancer[3]. A hallmark of exhausted CD8+ T cells is expression of various inhibitory receptors most notably PD-1[4]. Several studies have shown that the pool of exhausted CD8+ T cells is phenotypically and functionally heterogeneous[5–8]. Our goal here was to better characterize the CD8+ T cells that are present during chronic viral infection. A previous study shows that a subset of human CD8+ T cells express CXCR5[9], a chemokine receptor, that is normally present on B cells and CD4+ T_{FH} cells. Another study described CXCR5+ CD8+ T cells that regulate autoimmunity in mice[10]. We therefore investigated whether CXCR5+ CD8+ T cells were also generated during persistent viral infections. We addressed this issue using the mouse model of LCMV infection in which T cell exhaustion was first documented[1]. We found that there was a distinct population of CXCR5+ LCMV glycoprotein 33–41 epitope (GP33)-specific CD8+ T cells in the spleens of chronically infected mice (LCMV clone 13 strain), whereas GP33-specific memory CD8+ T cells in mice that had cleared the infection (LCMV Armstrong strain) did not express CXCR5 (Fig. 1a). The CXCR5+ CD8+ T cells in chronically infected mice also expressed the CD4+ T_{FH} markers ICOS and Bcl-6 and were negative for Tim-3, a marker associated with CD4+ T_H1 cells[11]. In contrast, the CXCR5− GP33-specific CD8+ T cells in chronically infected mice expressed Tim-3 and were negative for ICOS and Bcl-6. Both subsets of GP33-specific CD8+ T cells in chronically infected mice expressed high levels of the PD-1 inhibitory receptor, with the CXCR5− cells showing slightly higher levels (Fig. 1a). An identical pattern of expression of these molecules was seen with CD8+ T cells that recognize another LCMV epitope, GP276 (Extended Data Fig. 1a). Thus, this novel population of CXCR5+ cells was seen with both tetramer positive CD8+ T cells and these cells were detectable as early as day 8 after infection and were stably maintained in mice with high levels of viremia (Fig. 1b, Extended Data Fig. 1b). To determine if the generation of these cells was due to antigen persistence or to the different tropism of LCMV clone 13[12], mice were infected with either a low dose (2×10^2 plaque-forming units (PFU)) of clone 13 that is controlled within a week, or with a high dose (2×10^6 PFU) that causes a persistent infection. CXCR5+ LCMV-specific CD8+ T cells were only generated in the chronically infected mice, showing

that antigen persistence drives the generation of this CD8$^+$ T cell subset (Extended Data Fig. 2).

Transcriptional profiling revealed that the PD-1$^+$CXCR5$^+$ and PD-1$^+$CXCR5$^-$ CD8$^+$ T cells in chronically infected mice had distinct gene signatures (Extended Data Fig. 3a). Notably, the CXCR5$^+$ CD8$^+$ T cells expressed higher levels of several costimulatory molecules (*Cd28, Icos, Tnfsf14* (LIGHT), *Tnfrsf4* (OX-40)) and lower levels of inhibitory receptors (*Cd244* (2B4), *Havcr2* (Tim-3), *Entpd1* (CD39), *Lag3*) compared to CXCR5$^-$ cells (Fig. 1c, Extended Data Fig. 3b). These two CD8$^+$ T cell populations also showed differences in the expression of effector molecules, chemokines and chemokine receptors, Toll-like receptors (TLRs), transcription factors and memory markers (Fig. 1c and Extended Data Fig. 3b). CXCR5$^-$ CD8$^+$ T cells had higher levels of several effector molecules (perforin, granzymes, etc.), but did not express IL-2 or TNF, suggesting a more terminally differentiated state (Fig. 1c, Extended Data Fig. 4), confirming and extending earlier results with PD-1$^+$Tim-3$^+$ CD8$^+$ T cells[7]. Interestingly, the two CD8$^+$ T cell subsets expressed different *Tlr* genes (Fig. 1c). TLRs are key molecules associated with innate immune responses but their role on CD8$^+$ T cells is not well understood[13]. *Tlr3* and *Tlr7* were selectively upregulated by CXCR5$^+$ CD8$^+$ T cells and this was corroborated by enrichment of TLR cascade genes and interferon signalling pathways in this subset (Extended Data Fig. 5a). Regarding transcription factors, the CXCR5$^+$ CD8$^+$ T cells expressed *Bcl6, Tcf7* and *Plagl1* that are typically associated with CD4$^+$ T_{FH} cells[14], whereas CXCR5$^-$ cells expressed *Prdm1* (Blimp-1) that is linked with CD4$^+$ T_H1 cells and effector CD8$^+$ T cells, highlighting the distinct transcriptional fates of these two CD8$^+$ T cell subsets. Both subsets expressed *Eomes* and *Tbx21* (T-bet) but CXCR5$^+$ cells showed higher *Eomes* and lower *Tbx21* expression. The expression pattern of *Id2* and *Id3* was informative; the CXCR5$^-$ cells had high Id2 and low Id3 pattern found in terminal effector CD8$^+$ T cells that mostly die whereas CXCR5$^+$ CD8$^+$ T cells had low *Id2* and high *Id3*, the transcriptional profile characteristic of memory precursor CD8$^+$ T cells that survive and give rise to the pool of long-lived memory cells[15]. The expression of memory cell markers *Sell* (CD62L) and *Il7r* (CD127) was also consistent with the CXCR5$^+$ cells being less differentiated. In addition, the CXCR5$^+$ subset had enriched genes associated with mitochondrial fatty acid β-oxidation and mTOR signalling (Extended Data Fig. 5). Recent studies have highlighted the importance of fatty acid metabolism in maintenance of memory CD8$^+$ T cells[16,17]. Furthermore, CXCR5$^+$ CD8$^+$ T cells expressed several genes in the Wnt signalling pathway that are known to be associated with self-renewal and the maintenance of haematopoietic stem cells[18] (Fig. 1c). To determine if gene expression levels seen by microarray analysis correlated with protein expression, we co-stained CXCR5$^+$ and CXCR5$^-$ GP33-specific and GP276-specific CD8$^+$ T cells with a representative set of markers and found that there was an excellent correlation between RNA levels and protein expression (Fig. 1d, Extended Data Fig. 1c). Gene set enrichment analysis (GSEA) showed that CXCR5$^-$ CD8$^+$ T cells were related to CD4$^+$ T_H1 cells and CD8$^+$ terminal effectors, whereas the CXCR5$^+$ subset was similar to CD4$^+$ T_{FH} cells and CD8$^+$ memory precursors (Fig. 1e, Extended Data Fig. 6). Interestingly, we also found a relationship between CXCR5$^+$ CD8$^+$ T cells and haematopoietic stem cell progenitors (Fig. 1e). Taken together, these results suggest that LCMV-specific CXCR5$^+$ CD8$^+$ T cells may function as memory stem cells during chronic infection.

LCMV clone 13 causes a disseminated infection that targets multiple lymphoid and non-lymphoid organs, so we next analysed the tissue distribution of the two $CD8^+$ T cell subsets in chronically infected mice. We found that LCMV-specific $CXCR5^+$ $CD8^+$ T cells were present only in lymphoid tissues whereas the more terminally differentiated $CXCR5^-$ $CD8^+$ T cells were present in both lymphoid and non-lymphoid organs (Fig. 2a, Extended Data Fig. 7a,b). The blood presented a notable pattern; during the early phase (day 8) of chronic infection, both subsets were present in the blood, but later (day 30 onwards) only the $CXCR5^-$ $CD8^+$ T cells were in circulation (Extended Data Fig. 7c,d). As both $CD8^+$ T cell subsets were present in the spleen, we determined their anatomic location within the organ. We used multiplexed confocal imaging coupled with histocytometry analysis, a technique that simultaneously permits quantitative assessment of cellular phenotype and positioning in tissues[19]. Owing to lack of available CXCR5 antibodies capable of *in situ* staining of fixed mouse tissues, we identified the two $CD8^+$ T cell subsets based on expression of TCF1. The $CXCR5^+Tim\text{-}3^-$ subset is $TCF1^+$ whereas the $CXCR5^-Tim\text{-}3^+$ cells are $TCF1^-$ (Fig. 1d). Naïve $CD8^+$ T cells also express TCF1 so we used the PD-1 stain to discriminate between naïve cells ($PD\text{-}1^-$) and the two $CD8^+$ T cell subsets from chronically infected mice (both $PD\text{-}1^+$) (Extended Data Fig. 8a). Quantitative analysis showed that the $CXCR5^+$ $CD8^+$ T cell subset was present predominantly in the T cell zones of the white pulp (along with naïve T cells) whereas the $CXCR5^-$ subset was located mostly in the red pulp of the spleen (Fig. 2b–d). Similar results were observed when we examined the anatomic location of the two subsets in the spleen at an earlier time after infection (Extended Data Fig. 8b,c). In this context it is worth noting that the red pulp is the major site of LCMV infection in the spleen and this is where the more terminally differentiated $CD8^+$ T cells reside[20] (Extended Data Fig. 8d). There are also some LCMV-infected cells in the white pulp (dendritic cells and fibroblastic reticular cells) but the red pulp macrophages are the major reservoir of infection in the spleen[21]. We next performed *in vivo* intravascular labelling[22] using injection of fluorophore-conjugated anti-CD45.2 to further confirm the differential distribution of $CXCR5^+$ and $CXCR5^-$ $CD8^+$ T cells into the T cell zone and red pulp, respectively. We found that most of the $CXCR5^-$ $CD8^+$ T cells were stained by the *in vivo* antibody, showing their access to the blood in the red pulp, whereas the $CXCR5^+$ $CD8^+$ T cells were not stained by the intravascular staining consistent with their preferential localization in the splenic white pulp (Fig. 2e). Notably, the $CXCR5^+$ $CD8^+$ T cells were located predominantly in the T cell zones and not in the B cell areas. This was despite the fact that the CXCR5 molecule on these cells was functional and these $CD8^+$ T cells were able to migrate in response to the chemokine CXCL13 in an *in vitro* assay (Extended Data Fig. 8e,f). However, the $CXCR5^+$ $CD8^+$ T cells also expressed higher levels of *Ccr7* mRNA compared to their $CXCR5^-$ counterparts and were able to migrate in response to the chemokines CCL19/21 that are present in the T cell areas (Fig. 2f,g). This functional CCR7 could explain the positioning of this $CXCR5^+$ $CD8^+$ T cell subset in the T cell zone[23]. The $CXCR5^+$ $CD8^+$ T cells also expressed higher levels of CD69 (Fig. 2h). This could also contribute to their retention in the T cell areas[24]. Finally, the $CXCR5^+$ $CD8^+$ T cells express very high levels of the chemokine-encoding gene *Xcl1* that promotes interactions with $XCR1^+$ lymphoid dendritic cells that are predominantly located in the white pulp[25] (Fig. 1c).

To examine the *in vivo* dynamics of the two CD8$^+$ T cell subsets, we transferred congenically marked Cell-trace Violet (CTV)-labelled CXCR5$^+$Tim-3$^-$ and CXCR5$^-$Tim-3$^+$ cells from chronically infected mice into infection-matched recipients (Fig. 3a). As shown in Fig. 3b, the CXCR5$^-$ CD8$^+$ T cells exhibited minimal to no division in the spleen or liver of recipient mice 21 days after transfer and these cells also retained their phenotype. In contrast, the CXCR5$^+$ CD8$^+$ T cells not only underwent proliferation resulting in self-renewal but also gave rise to the CXCR5$^-$Tim-3$^+$ subset. Consistent with this, there was a higher frequency of donor cells in the spleens of recipient mice that received CXCR5$^+$ CD8$^+$ T cells (Fig. 3c). These results show that CXCR5$^-$ CD8$^+$ T cells are terminally differentiated with limited proliferative potential, whereas the CXCR5$^+$ CD8$^+$ T cells act as stem cells during chronic infection; they undergo a slow self-renewal and also give rise to the more terminally differentiated effector-like CD8$^+$ T cell subset that is present in both lymphoid and non-lymphoid tissues. We next tested the ability of CXCR5$^+$ and CXCR5$^-$ CD8$^+$ T cell subsets to respond to LCMV clone 13 infection after transfer into naïve mice. These experiments were performed after transfer of low numbers (2,500) or high numbers (90,000) of donor cells (Extended Data Fig. 9a). Identical results were seen in both conditions. The transferred CXCR5$^-$ CD8$^+$ T cells showed no expansion in the blood, spleen or liver, but there was vigorous expansion of the transferred CXCR5$^+$ CD8$^+$ T cells in all of these tissues (Fig. 3d, Extended Data Fig. 9b–h). In addition, CXCR5$^+$ cells once again gave rise to both the CXCR5$^+$ and CXCR5$^-$ CD8$^+$ T cell subsets, which further documents their proliferative capacity and stem cell-like characteristics (Fig. 3e, Extended Data Fig. 9d,g).

PD-1 is a central regulator of CD8$^+$ T cell exhaustion and blockade of this inhibitory pathway enhances T cell immunity in chronic viral infections and cancer[3,4]. To determine how these two CD8$^+$ T cell subsets would respond to PD-1 blockade, CXCR5$^+$ and CXCR5$^-$ CD8$^+$ T cells were transferred into infection-matched chronically infected mice and groups of these mice were then treated with PD-L1 blocking antibody (Extended Data Fig. 10a). Blockade of the PD-1 inhibitory pathway had minimal effect on CXCR5$^-$ CD8$^+$ T cells. In contrast, the CXCR5$^+$ CD8$^+$ T cells responded to the PD-1 blockade and were present in significantly higher numbers in mice that were treated with the anti-PD-L1 antibody (Fig. 3f). PD-1 blockade substantially increased (>30-fold) the differentiation of CXCR5$^+$ CD8$^+$ T cells into the CXCR5$^-$ CD8$^+$ T cell subset (Fig. 3g, Extended Data Fig. 10b). These results show that the proliferative burst seen after PD-1 blockade comes from this novel PD-1$^+$ CD8$^+$ T cell subset that we have identified.

The marked difference in the expression of TCF1 between the CXCR5$^+$ and CXCR5$^-$ CD8$^+$ T cell subsets (Fig. 1d) was of interest, as recent studies have shown that this transcription factor plays a role in the generation of CD4$^+$ T_{FH} cells[26,27] and also in the maintenance of haematopoietic stem cells in an undifferentiated state[28]. We examined the role of TCF1 (encoded by *Tcf7*) in the generation of this CXCR5$^+$ CD8$^+$ T cell subset using *Tcf7*-deficient P14 transgenic CD8$^+$ T cells that recognize the GP33 epitope from LCMV glycoprotein. Wild-type or *Tcf7*$^{-/-}$ P14 cells were transferred into congenically distinct naïve mice followed by LCMV clone 13 infection (Fig. 4a). The *Tcf7*$^{-/-}$ P14 cells expanded after clone 13 infection, but exhibited a notable defect in their ability to generate CXCR5$^+$Tim-3$^-$ CD8$^+$ T cells whereas wild-type P14 cells gave rise to both CXCR5$^+$ and CXCR5$^-$ CD8$^+$ T cells as expected (Fig. 4b,c,e). Endogenous GP33-specific CD8$^+$ T cells in

mice that received *Tcf7*$^{-/-}$ P14 cells also differentiated normally into both CD8$^+$ T cell subsets (Fig. 4d). Taken together, these results show that TCF1 has an essential and cell intrinsic role in the differentiation of CXCR5$^+$ CD8$^+$ T cells. The inability to generate this CD8$^+$ T cell subset was coupled to a marked loss of the *Tcf7*$^{-/-}$ P14 cells from both lymphoid and non-lymphoid tissues (Fig. 4f–i). In summary, these data show that TCF1 is indispensable for the generation of CXCR5$^+$ CD8$^+$ T cells and that these stem-like cells are critical for the maintenance of virus-specific CD8$^+$ T cells during chronic infection.

We have defined a PD-1$^+$ virus-specific CD8$^+$ T cell population in chronically infected mice that is characterized by a unique gene signature with similarities to CD4$^+$ T_{FH} cells, CD8$^+$ memory precursor cells and haematopoietic stem cell progenitors. This unique transcriptional program may represent a specific adaptation of CD8$^+$ T cells to chronic antigenic stimulation. It will be of interest to determine if a similar adaptation occurs during autoimmunity and cancer. The identification of such CD8$^+$ T cells in cancer will be of special relevance as our studies in chronic LCMV infection have shown that these CD8$^+$ T cells selectively proliferate after PD-1 blockade. PD-1 directed immunotherapy is now one of the most promising approaches for treatment of several different types of cancers and is an approved drug for melanoma, lung cancer and bladder cancer. Our study, defining the phenotype and gene expression program of the CD8$^+$ T cells that respond to PD-1 blockade, should facilitate the rational design of combination immune therapies.

Methods

Mice, viral infections and virus titration

Six to eight-week-old female C57BL/6 mice and CD45.1 congenic mice were purchased from Jackson Laboratory. Mice were infected with either LCMV Armstrong strain (2×10^5 PFU, intraperitoneally(i.p.)), low dose LCMV clone 13 strain (2×10^2 PFU, intravenously (i.v.)) for acute infections, or high dose LCMV clone 13 strain (2×10^6 PFU, i.v.) for chronic infections. Additionally, transient CD4$^+$ T cell depletion was used in the chronic LCMV infection model to induce life-long systemic infection with high levels of viremia, which provides an optimal model to study T cell exhaustion[29]. Serum viral titers were determined by plaque assay on Vero E6 cells as described previously[30]. The conditional knockout P14 female mice for *Tcf7* were Rosa26^{GFP} *Tcf7*$^{fl/fl}$hCD2-Cre$^+$ (referred to as '*Tcf7*$^{-/-}$') in which 80–90% of peripheral T cells had deletion of *Tcf7* with GFP expression representing Cre recombinase activity[27]. Littermate Rosa26^{GFP} *Tcf7*$^{fl/fl}$hCD2-Cre$^-$ P14 mice were used as wild-type control mice. LCMV D^{b}GP33-specific TCR transgenic P14 mice were fully backcrossed to C56BL/6 mice. No statistical methods were used to predetermine sample size. The number of animals for each experiment was determined based on previous experience with the model system. The investigators were not blinded to allocation during experiments and outcome assessment and the experiments were not randomized. All animal experiments were performed in accordance with Emory University Institutional Animal Care and Use Committee.

Flow cytometry

Flow cytometric analysis was performed on a FACS Canto II or LSR II (BD Biosciences). Lymphocytes were isolated from tissues including spleen, blood, liver, bone marrow, brain, gut intestinal epithelium, and mesenteric lymph nodes as described previously[30,31]. Direct *ex vivo* staining and intracellular cytokine staining were performed as described previously[30] with fluorochome-conjugated antibodies (purchased from BD Bioscience, eBioscience, BioLegend, R&D, Cell Signaling Technology, Vector Laboratories, and Invitrogen). To detect LCMV-specific $CD8^+$ T cell responses, tetramers were prepared as described previously[32]. For detection of CXCR5, a three-step staining protocol was used as described previously[33] with minor modifications. Cells were stained with tetramer and rat anti-mouse CXCR5 antibody (BD Bioscience). Samples were then incubated with 20 μM d-biotin (Avidity) and a secondary biotin-SP-conjugated Affinipure $F(Ab')_2$ goat anti-rat IgG (Jackson Immunoresearch). Finally, cells were stained with streptavidin-APC (Invitrogen), streptavidin-PE or streptavidin-BV421 (BioLegend) as well as with antibodies specific to surface molecules. Note that collagenase digestion resulted in reduced staining for CXCR5. For intracellular detection of transcription factors such as Bcl-6, T-bet, Eomes and TCF1, surface-stained cells were permeabilized, fixed and stained by using the Foxp3 Permeabilization/Fixation Kit according to manufacturer's instructions (eBioscience). For intracellular detection of pS6, surface-stained cells were permeabilized, fixed and stained using Phosflow Lyse/Fix buffer (BD) and Phosflow Perm/Wash buffer I (BD). For *in vivo* antibody labelling, 30 μg of BV421-conjugated anti-CD45.2 antibody (BioLegend) was injected i.v. into chronically infected mice. Three minutes after the injection, splenocytes were isolated and used for direct *ex vivo* staining as described previously[22]. FACS data were analysed with FlowJo software (TreeStar).

wCell sorting was performed on a FACS Aria II (BD Biosciences). Microarray analysis, *in vitro* chemotaxis, and transfer experiments were performed on PD-1^+CXCR5^+Tim-3^- and PD-1^+CXCR5^-Tim-3^+ $CD8^+$ T cells sorted from chronically infected mice (>45 days p.i.) at a purity of greater than 96%. $CD44^{lo}CD8^+$ T cells and $B220^+CD19^+$ B cells were isolated from uninfected mice.

RNA isolation and microarray analysis

RNA from sorted cells was purified (QIAGEN) and hybridized to Affymetrix mouse 430 2.0 arrays (Memorial Sloan-Kettering Cancer Center, Genomics Core Facility). Raw data (CEL files) were normalized by RMA using Affy R package. Principal component analysis was performed using arrayQualityMetrics R package. Differential expression analysis was performed between any two subsets using limma R package (Adjusted P-value < 0.05 and fold-change > 1.5). Gene Set Enrichment Analysis (GSEA) was run for each cell subset in pre-ranked list mode with 1,000 permutations (nominal P-value cutoff < 0.01). As gene sets for the GSEA analyses, we used Reactome pathways (http://www.reactome.org/); the MSigDB gene sets related to haematopoietic stem cells[34]; and gene signatures associated with T_{FH} or T_H1 $CD4^+$ T cells[33], memory precursor/terminal effector $CD8^+$ T cells[35] and thymic innate T_{FH}-like $CD4^+$ T cells[36]. To define these signatures, we downloaded the microarray data from GEO database (GSE16697, GSE8678 and GSE64779); collapsed probe sets that matched to the same gene symbol by taking the one with highest expression

across all samples; removed genes with lowest 30% mean expression; and performed differential expression analysis between the two classes using limma (adjusted P-value < 0.01 and fold-change > 2). Enrichment scores were visualized using the corrplot package in R. Enrichment scores of Reactome pathways and the genes shared by two pathways were represented as nodes and links, respectively using Cytoscape software. The microarray data are available in the Gene Expression Omnibus (GEO) database (http://www.ncbi.nlm.nih.gov/geo) under the accession number GSE84105.

Confocal microscopy and histocytometry

To examine the localization of the $CD8^+$ T cell subsets in the spleen, 20 μm paraformaldehyde-fixed paraffin-embedded spleen sections were prepared, imaged, and analysed as previously described with minor modifications[19]. Briefly, images were acquired with a Lecia SP8 tiling confocal microscope (Leica Microsystems) equipped with a 40× 1.3NA oil objective. Fluorophore spillover into adjacent channels was compensated using the Leica Channel Dye Separation module. Owing to high spatial resolution of the objective, deconvolution was not performed. Nuclear histo-cytometry analysis was performed by segmentation of all Jojo-1 stained nuclei (1:15,000 dilution; Invitrogen) in the imaged volume using Imaris (Bitplane) surface creation module, and by exporting the resultant statistical information into Excel (Microsoft) and then into Flowjo 10 (TreeStar). Positional gates for the T-cell zones, B-cell follicles and the red pulp were created in Flowjo using the relative densities of $CD3^+B220^-$ T cells, $CD3^-B220^+$ B cells and $CD3^-B220^-CD44^{hi}$ myeloid cells, respectively. These gates were then applied to the cells of interest to assess their relative distribution across different splenic compartments.

To examine which area of the spleen is infected by LCMV clone 13, spleens of chronically infected mice (>45 days p.i.) were isolated and embedded in OCT-Tissue Tek and frozen immediately over liquid-nitrogen-chilled isopentane. Sections 7 μm in thickness were cut using a micro-cryotome. They were air-dried, and then fixed in chilled acetone:methanol (1:1, v/v) at −20 °C for 10 min. The slides were permeabilized in 0.1% Triton X-100 for 30 min. The spleens were blocked with goat serum, mouse Fc block (clone 2.4G2, BD Bioscience) and avidin-biotin blocking reagent (Vectashield). The slides were then stained for LCMV antigen using pig anti-LCMV sera (1:200), BV421-rat anti-IgD (1:200, BioLegend) and biotin hamster anti-CD3 (1:100, BD Bioscience) for 1 h, followed by Alexa 555 anti-pig IgG (1:500, Invitrogen) and streptavidin –Alexa 647 (1:200, BioLegend). After washing with PBS, the slides were mounted with Prolong Gold mounting medium (Life Technologies) and cover slipped. The pictures were taken using AxioCam MRc (Zeiss) with Axionvision Rel4.7 software.

Chemotaxis

Chemotaxis assays were performed as described previously[37] with minor modifications. Transwells with 5 μm pores (Corning Costar) were used. Sorted $CXCR5^+$ and $CXCR5^-$ $CD8^+$ T cells (2.5×10^4 cells in 100 μl) were seeded onto upper wells. The bottom wells contained either 580 μl of PBS, a mixture of recombinant CCL19 and CCL21 (each 1 μg/ml, R&D), or recombinant CXCL13 (3 μg/ml, R&D). Transmigrated cells were counted by flow

cytometry for 200s at medium acquisition speed. The chemotactic index represents the ratio of cells in the lower chamber in the presence versus absence of chemokines.

Cell transfer, labelling with cell tracking dye and PD-1 blockade

For adoptive transfer experiments, 2.5×10^3 or 0.6 to 1.0×10^5 $CD8^+$ T cells sorted from the spleens of chronically infected mice (>45 days p.i.) were transferred i.v. into infection-matched, or naïve mice. To track the proliferation of lymphocytes, sorted $CD8^+$ T cells were labelled with Cell-trace Violet (Invitrogen), according to the manufacturer's protocol. PD-1 blockade was performed as described previously[4] after the transfer of two $CD8^+$ T cell subsets into infection-matched mice. For P14 experiments, splenocytes containing 2.5×10^3 wild-type or *Tcf7*$^{-/-}$ P14 cells ($CD45.2^+$) were transferred i.v. into naïve CD45.1 recipient mice.

Statistical analysis

All experiments were analysed using Prism 6 (GraphPad Software). Statistical differences were assessed using a two-tailed unpaired or paired Student's t-test. P values of <0.05 and <0.01 indicated the significant difference between relevant groups.

Extended Data

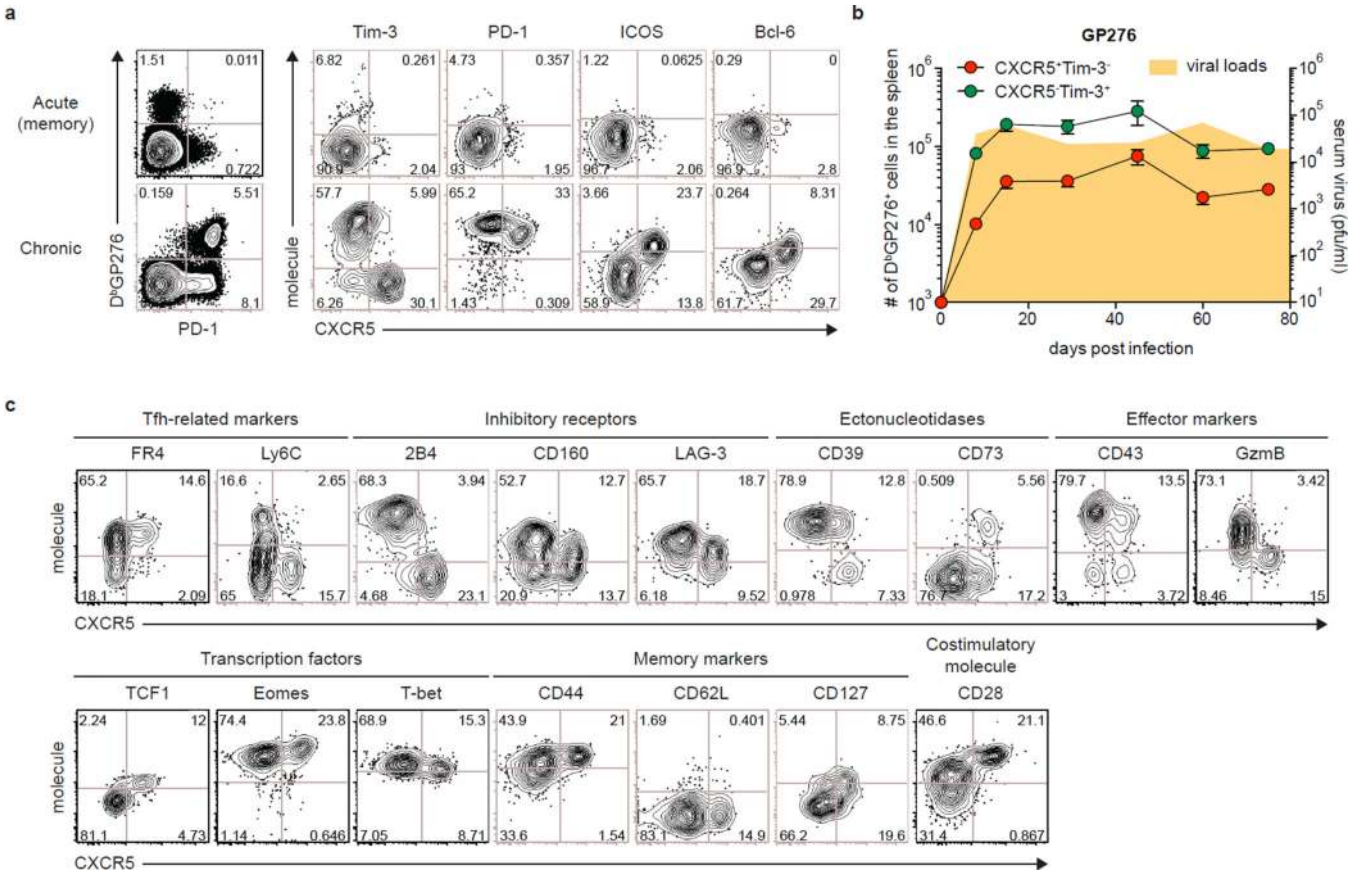

Extended Data Figure 1. LCMV GP276-specific $CD8^+$ T cells also consist of $CXCR5^+$ and $CXCR5^-$ $CD8^+$ T cell subsets during chronic infection

a, Phenotypic analysis of GP276-specific CD8$^+$ T cells in the spleens of immune mice that had cleared an acute LCMV Armstrong infection or mice that were chronically infected with LCMV clone 13 (day 30 after infection (p.i.)). FACS plots showing CXCR5 expression in combination with the indicated markers are gated on GP276 tetramer$^+$ CD8$^+$ T cells. **b**, Longitudinal analysis of the numbers of GP276-specific CXCR5$^+$Tim-3$^-$ and CXCR5$^-$Tim-3$^+$ CD8$^+$ T cells in the spleen at the indicated time after infection. LCMV titers in the serum are shown as the shaded yellow area. Graph shows the mean ± s.e.m. Data are the average of 8 mice from two experiments per time point (total n=48). **c**, Phenotypic characterization of CXCR5$^+$ and CXCR5$^-$ GP276-specific CD8$^+$ T cells in the spleen of chronically infected mice (>45 days p.i.).

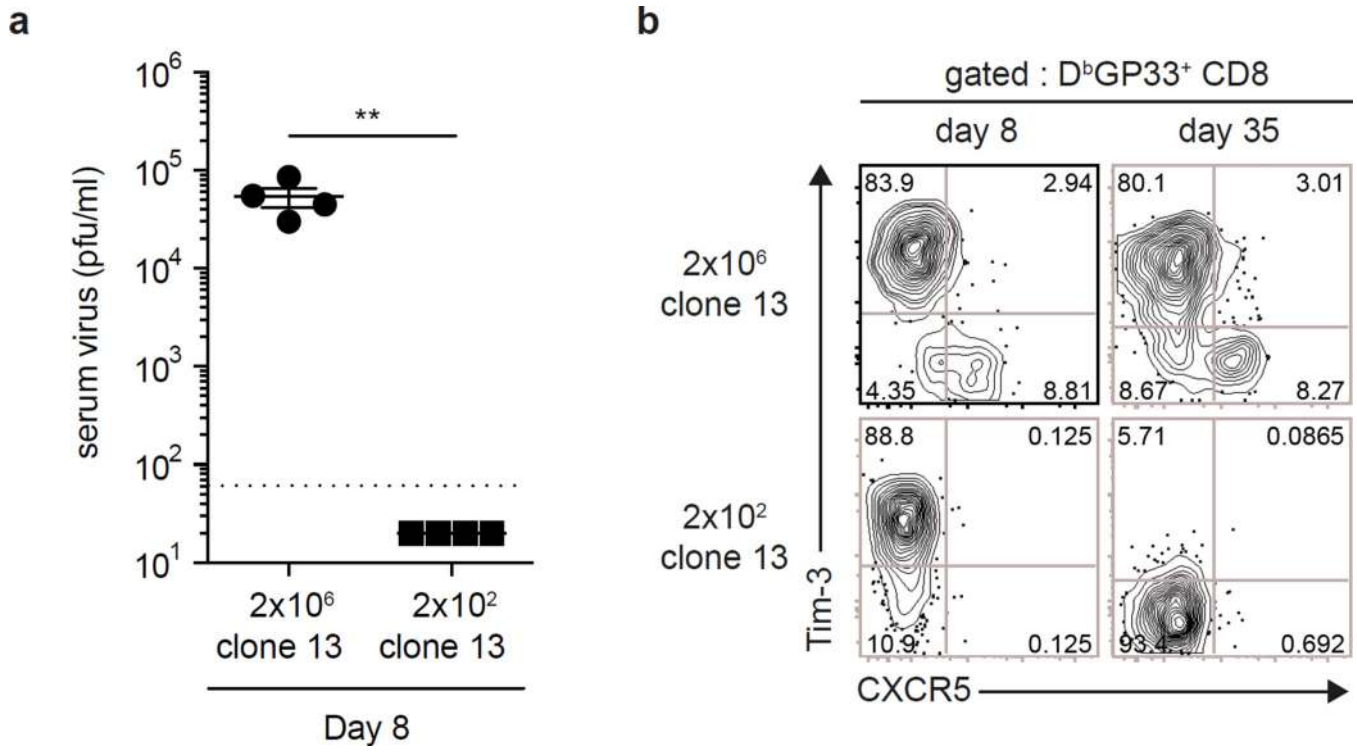

Extended Data Figure 2. Low dose challenge with LCMV clone 13 results in acute infection and does not generate CXCR5$^+$ CD8$^+$ T cells

Mice were infected with either low dose (2×10^2 PFU) or high dose (2×10^6 PFU) of LCMV clone 13, and the generation of CXCR5$^+$ CD8$^+$ T cells was examined at day 8 and day 35 p.i. **a**, Serum virus titers at day 8 after infection. **b**, Representative flow plots of CXCR5 and Tim-3 expression on GP33-specific CD8$^+$ T cells in the spleen at day 8 and 35 p.i. Data are obtained from a total of 16 mice with 4 mice per group at each time point. Student's t-test, where ** $P < 0.01$.

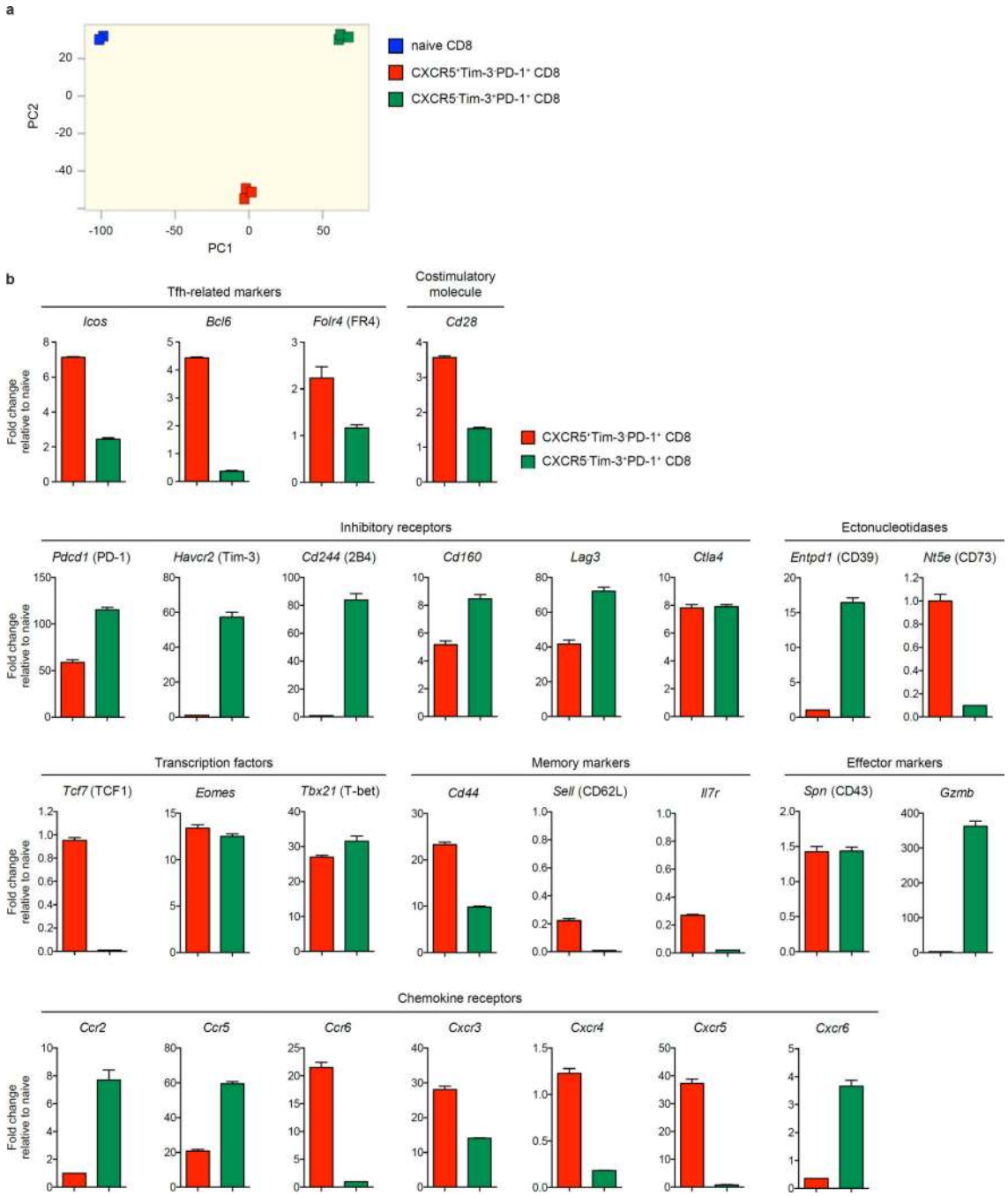

Extended Data Figure 3. Distinct transcriptional profiles of CXCR5^{+} and CXCR5^{-} CD8^{+} T cells from spleens of mice chronically infected with LCMV

a, Principal component analysis of naïve (CD44^{lo}) CD8^{+} T cells isolated from uninfected mice and CXCR5^{+}Tim-3^{-}PD-1^{+} and CXCR5^{-}Tim-3^{+}PD-1^{+} CD8^{+} T cells isolated from chronically infected mice (>45 days p.i.). Each square represents an individual biological replicate. **b**, Relative expression of selected genes as determined by Affymetrix microarray analysis. Data are shown as fold change relative to naïve (CD44^{lo}) CD8^{+} T cells. Graphs show the mean ± s.e.m.

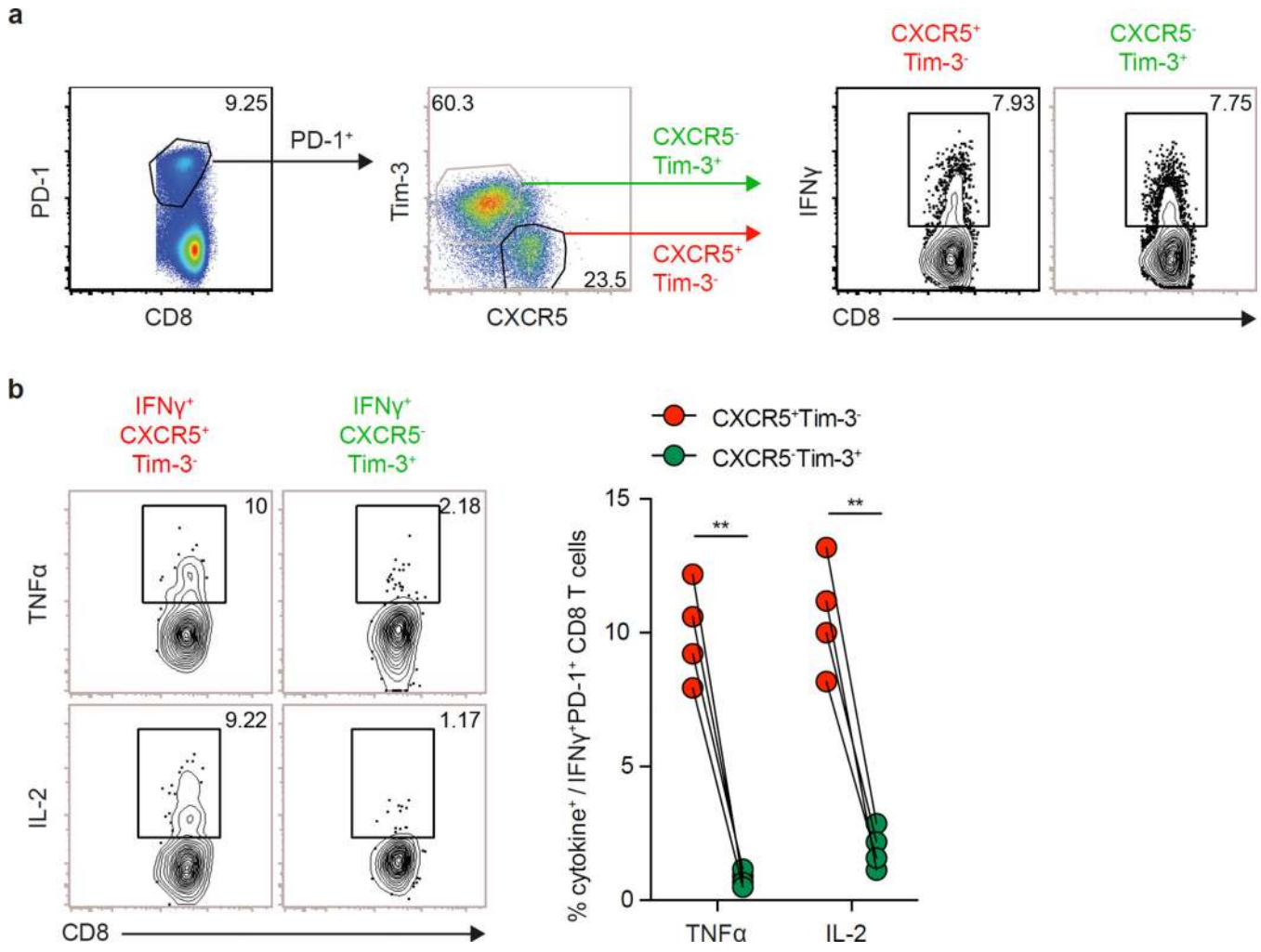

Extended Data Figure 4. LCMV-specific CXCR5$^+$ CD8$^+$ T cells are more polyfunctional than CXCR5$^-$ CD8$^+$ T cells

Splenocytes from chronically infected mice (>45 days p.i.) were stimulated with GP33–41 peptide for 5 h followed by phenotypic marker staining and intracellular staining. **a**, Gating strategy for IFNγ^+PD-1$^+$CXCR5$^+$Tim-3$^-$ and IFNγ^+PD-1$^+$CXCR5$^-$Tim-3$^+$ CD8$^+$ T cells. **b**, Representative FACS plots and graph showing the frequency of TNFα- and IL-2-producing cells among IFN-γ^+ CD8$^+$ T cells. Data are representative of 2 experiments (n=4 per experiment). Student's paired t-test, where ** $P < 0.01$.

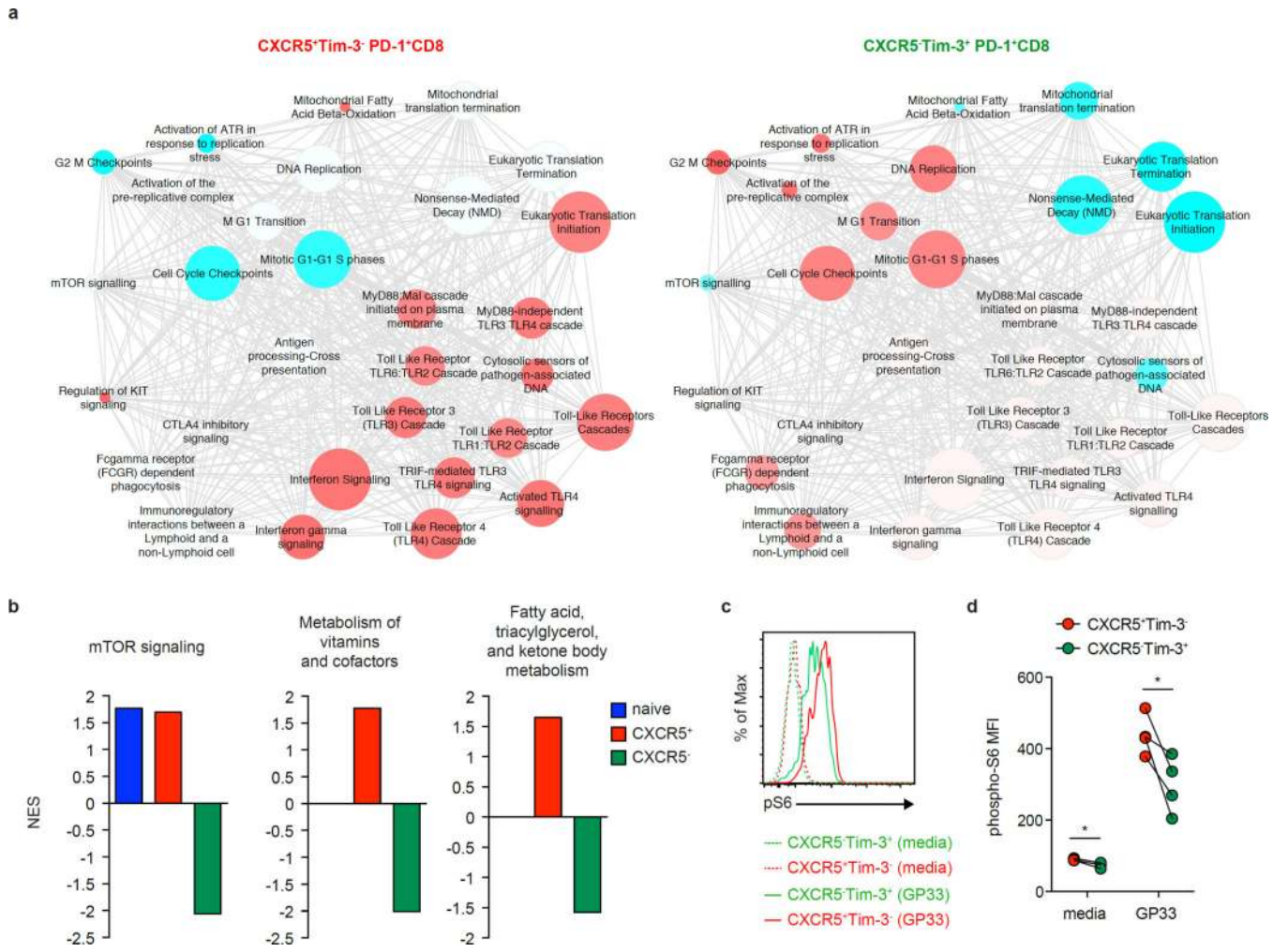

Extended Data Figure 5. Analysis of reactome pathways, mTOR signalling and fatty acid metabolism in CXCR5$^+$ and CXCR5$^-$ CD8$^+$ T cells from LCMV chronically infected mice

a. Reactome pathways in CXCR5$^+$Tim-3$^-$PD-1$^+$ and CXCR5$^-$Tim-3$^+$PD-1$^+$ CD8$^+$ T cells isolated from the spleens of mice chronically infected with LCMV (>45 days p.i.). GSEA (nominal P<0.01; 1,000 permutations) was used to identify positive (red, maximum normalized enrichment score (NES) = 3.2) or negative (blue, min NES = −3.7) enrichment of Reactome pathways (http://www.reactome.org/) in CXCR5$^+$Tim-3$^-$PD-1$^+$ and CXCR5$^-$Tim-3$^+$PD-1$^+$ CD8$^+$ T cells using meta-analysis. The size of the circles (nodes) represents the number of genes on each pathway. The links between circles (edges) represent the number of genes shared by two given pathways. The networks were generated using Cytoscape. **b**, GSEA on mTOR signalling and fatty acid metabolism. Bars represent pathways with nominal P-value < 0.01. **c,d,** Splenocytes from chronically infected mice (>45 days p.i.) were stimulated with medium or GP33–41 peptide for 1 h followed by phenotypic marker staining and phosphorylated S6 ribosomal protein (pS6) staining. Flow cytometry analysis (c) and MFI (d) of pS6 expression in CXCR5$^+$ and CXCR5$^-$ CD8$^+$ T cell subsets after *ex vivo* stimulation. Data are representative of 2 experiments (n=4 per experiment). Student's paired t-test, where * P < 0.05.

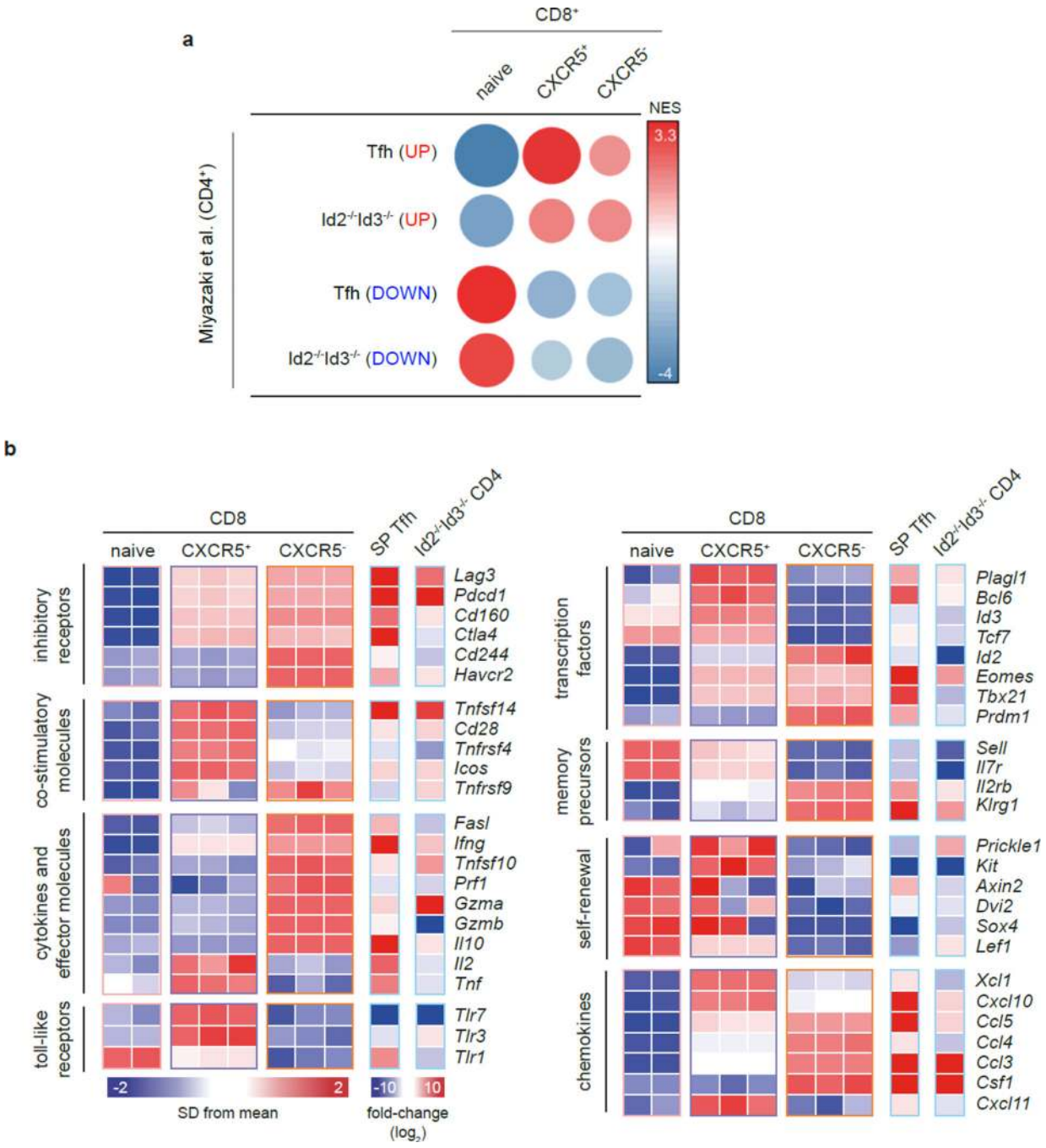

Extended Data Figure 6. Comparison of gene signatures of CXCR5$^+$ and CXCR5$^-$ CD8$^+$ T cell subsets from chronically infected mice with Id2$^{-/-}$Id3$^{-/-}$ innate T$_{FH}$-like CD4$^+$ T cells

a, GSEA was performed using genes pre-ranked by the mean Z-score values of each CD8$^+$ subset (naive, CXCR5$^+$ or CXCR5$^-$) calculated across all samples. Splenic CD4$^+$ T$_{FH}$ gene signatures from wild-type mice and thymic innate variant T$_{FH}$ gene signatures from Id2$^{-/-}$Id3$^{-/-}$ mice (GSE64779)[36] were used as gene sets in our GSEA. Genes were considered up- or downregulated in cell subsets compared to control (sorted CD4$^+$TCRβ$^+$CD8$^-$ cells) if there was a fold-change > 2 and P < 0.05[36]. **b**, Heat map

illustrating the relative expression of the indicated genes of $Id2^{-/-}Id3^{-/-}$ $CD4^+$ T cells defined in ref. 36 compared to those of naïve, $CXCR5^+$ and $CXCR5^-$ $CD8^+$ T cells. GSEA analysis revealed some interesting similarities and differences between the $CXCR5^+$ $CD8^+$ T cells from chronically infected mice and the $Id2^{-/-}Id3^{-/-}$ T_{FH}-like $CD4^+$ T cells. These two cell populations are distinct, but share certain biological properties such as increased self-renewal activity. For example, some of the interesting inhibitory and costimulatory molecules such as *Pdcd1* (PD-1), *Tnfsf14* (LIGHT), *Cd28*, and *Icos* were commonly upregulated in both $CXCR5^+$ $CD8^+$ and innate T_{FH}-like $CD4^+$ T cells, whereas molecules like *Cd244* (2B4), *Prf1, Fasl* and *Gzm*b were downregulated in both cell types. However, there were also many differences perhaps the most notable being the low expression of *Tcf7* (TCF1) in the innate $CD4^+$ T cells compared to the high expression of *Tcf7* in the $CXCR5^+$ $CD8^+$ T cells and the critical role of this transcription factor in the generation of these cells. Notably, the $CD4^+$ T cell population defined in ref. 36 is genetically deficient in both *Id2* and *Id3,* whereas the $CXCR5^+$ $CD8^+$ T cells express high levels of *Id3*. Thus, many aspects of the transcriptional program of these two cell types will be distinct.

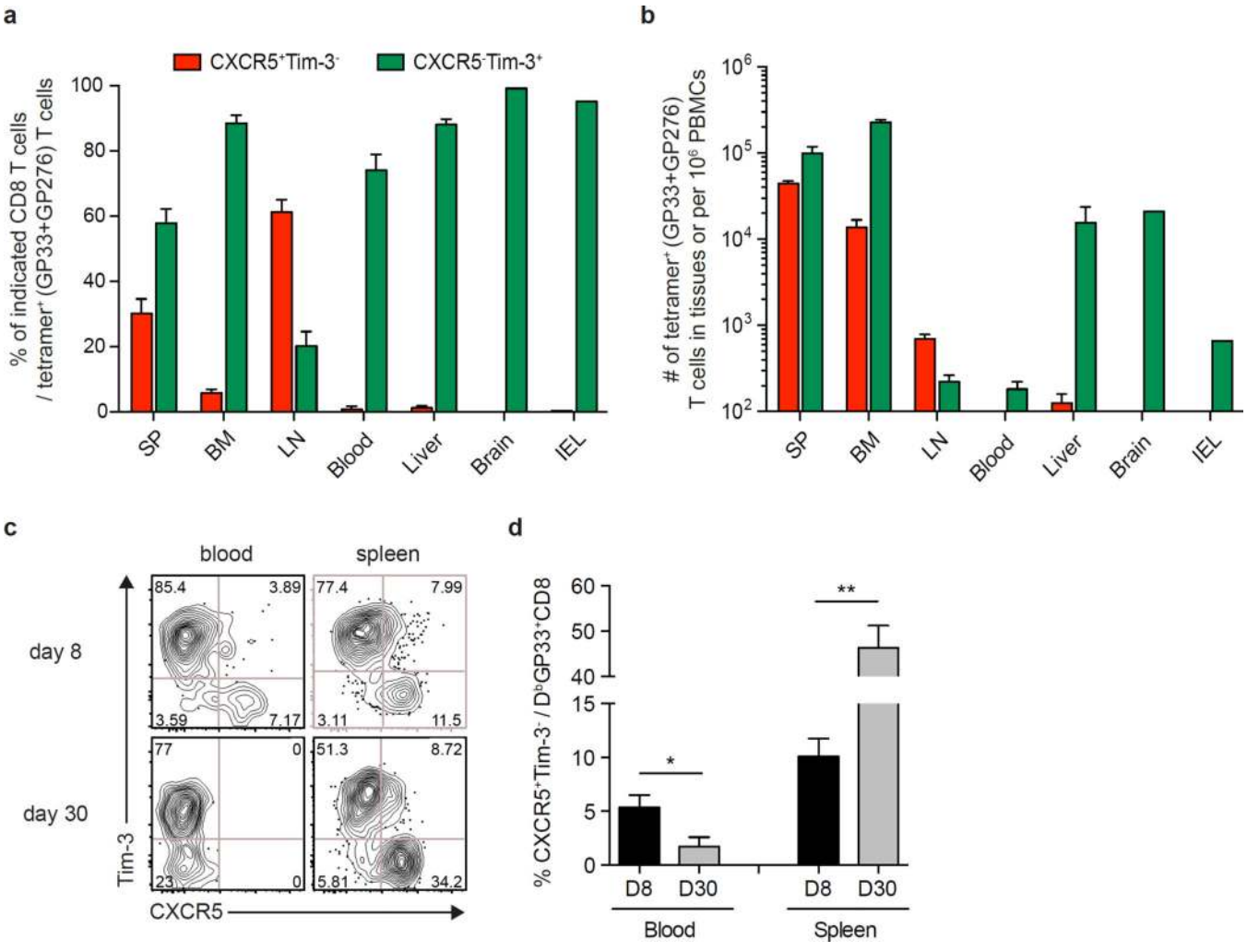

Extended Data Figure 7. Tissue distribution of LCMV-specific CXCR5^{+} and CXCR5^{-} CD8^{+} T cells in chronically infected mice

a,b, Frequency (a) and numbers (b) of LCMV-specific CXCR5^{+} and CXCR5^{-} CD8^{+} T cells in the indicated tissues at >45 days p.i. in chronically infected mice (SP, spleen; BM, bone marrow; LN, mesenteric lymph nodes; IEL, intestinal epithelial lymphocytes). **c,d,** Representative FACS plots (c) and graph (d) showing the frequency of CXCR5^{+}Tim-3^{-} GP33-specific CD8^{+} T cells in the blood and spleen at day 8 and day 30 p.i. FACS plots are gated on D^{b}GP33 tetramer^{+} CD8^{+} T cells. Data are obtained from 4 or 8 mice. Graphs show the mean ± s.e.m. Student's t-test, where **P < 0.01; *P < 0.05.

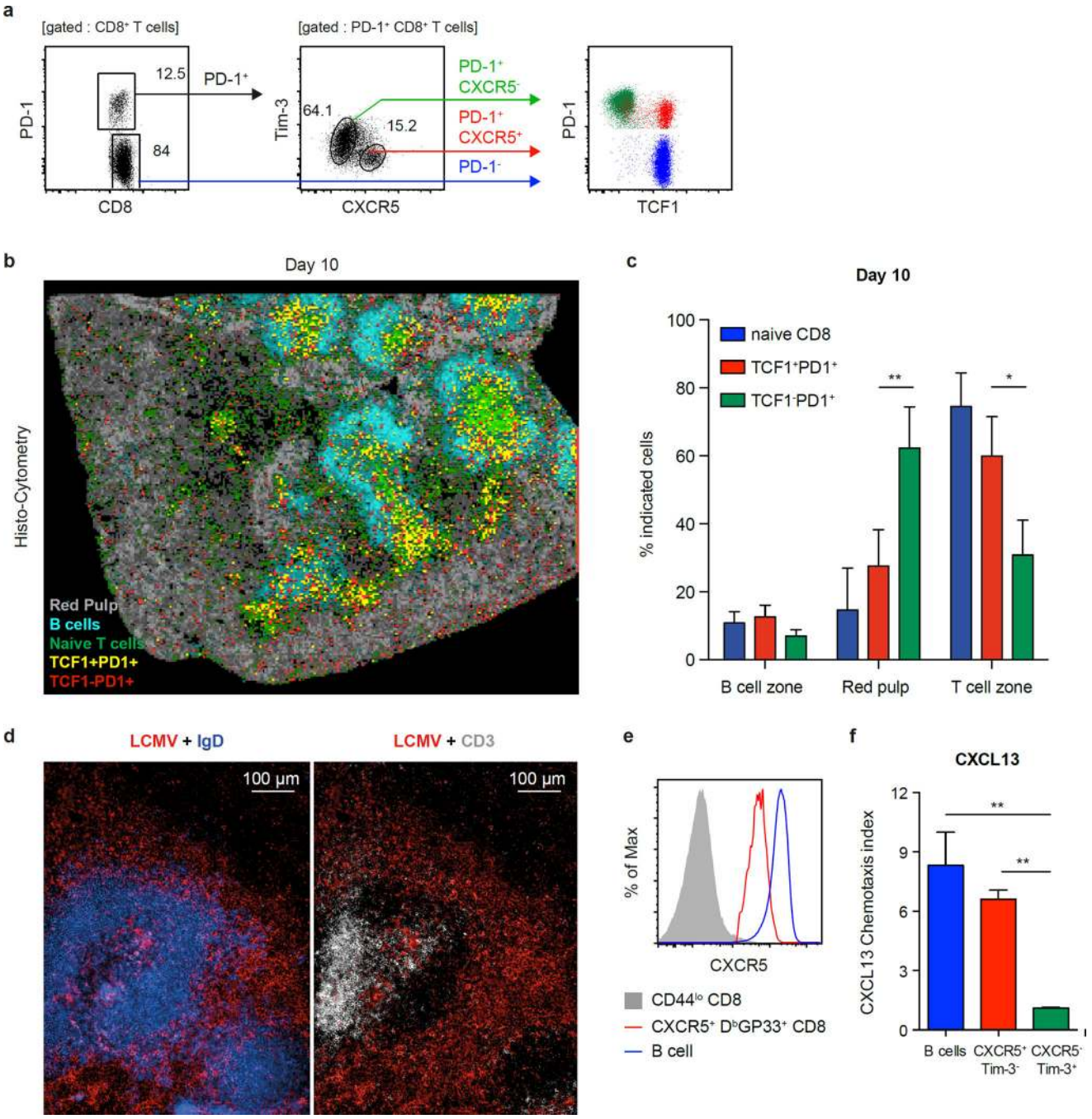

Extended Data Figure 8. Anatomic localization of CXCR5$^+$ and CXCR5$^-$ CD8$^+$ T cells in the spleen and *in vitro* migration of the two CD8$^+$ T cell subsets to CXCL13

a, Analysis of TCF-1 and PD-1 expression in CD8$^+$ T cell subsets in the spleen of chronically infected mice (>45 days p.i.). Left and middle FACS plots are gated on total CD8$^+$ T cells and PD-1$^+$ CD8$^+$ T cells, respectively. Right FACS plot displays the overlay of TCF-1 and PD-1 expression in gated PD-1$^-$, PD-1$^+$CXCR5$^+$Tim-3$^-$ and PD-1$^+$CXCR5$^-$Tim-3$^+$ CD8$^+$ T cells. **b,c,** Nuclear histocytometry analysis of the spleen (b) and frequency (c) of the CD8$^+$ T cell subsets within the respective zones of the spleen 10

days after LCMV clone 13 infection (n=3). **d**, Representative immunofluorescence staining of LCMV clone 13 infection in the spleen (>45 days p.i.). The spleen was stained for LCMV antigen (red), IgD (blue) and CD3 (white) and examined via microscopy (n=4). Note, LCMV infection is mostly in the red pulp. **e**, CXCR5 expression on splenic naïve ($CD44^{lo}$) $CD8^+$ T cells, B cells and $CXCR5^+$ GP33-specific $CD8^+$ T cells from chronically infected mice (>45 days p.i.). **f**, Relative migration of sorted B cells and $CXCR5^+Tim\text{-}3^-PD\text{-}1^+$ and $CXCR5^-Tim\text{-}3^+PD\text{-}1^+$ $CD8^+$ T cell subsets in response to CXCL13, which is a ligand for CXCR5. Data are combined from two experiments performed in duplicate wells for each sample. Graphs show the mean and s.e.m. Student's t-test, where $^{**}P < 0.01$; $^{*}P < 0.05$.

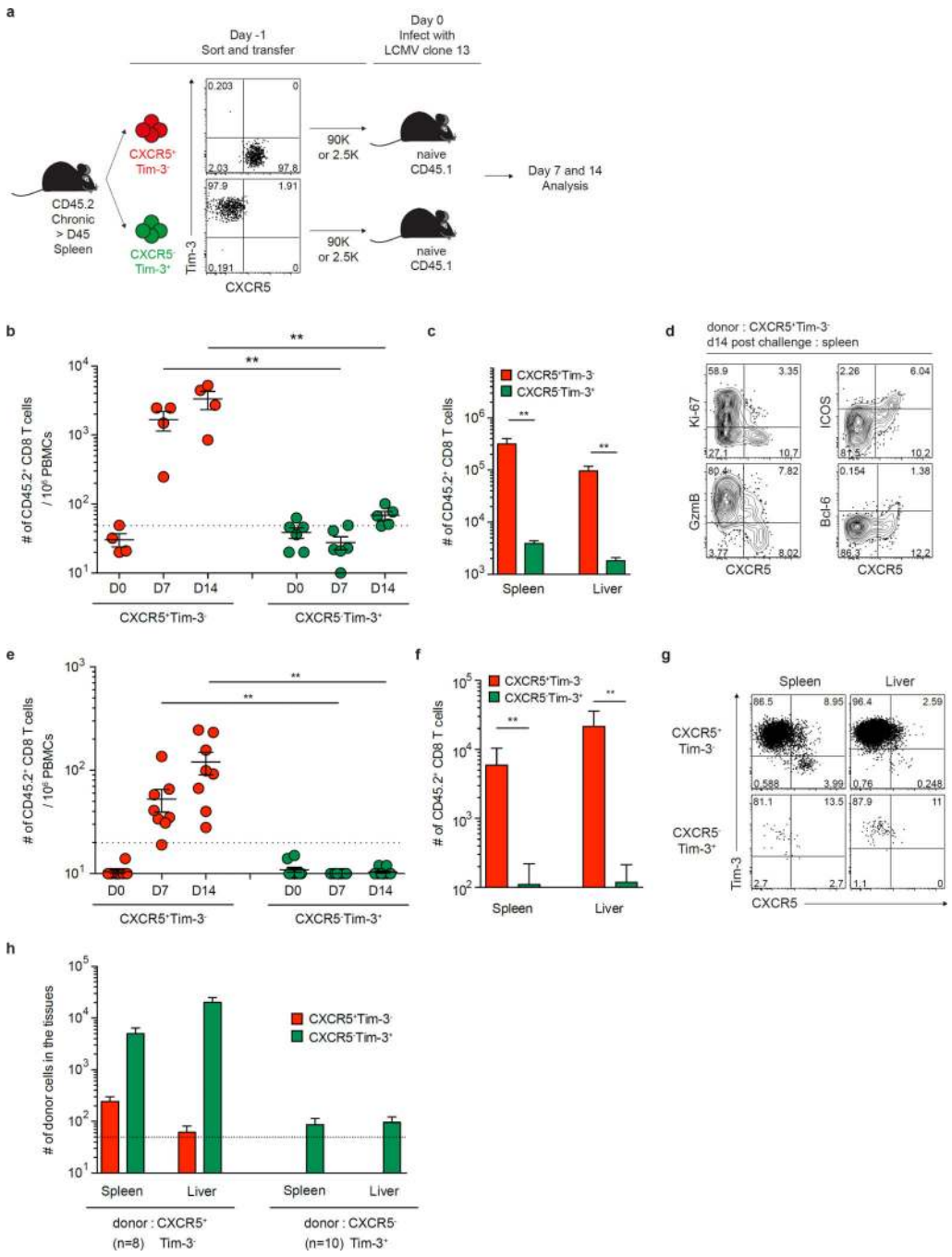

Extended Data Figure 9. CXCR5$^+$ CD8$^+$ T cells selectively undergo proliferation after LCMV clone 13 challenge

a, Sorted PD-1$^+$CXCR5$^+$Tim-3$^-$ and PD-1$^+$CXCR5$^-$Tim-3$^+$ CD8$^+$ T cells isolated from CD45.2$^+$ chronically infected mice (>45 days p.i.) were adoptively transferred into naive CD45.1$^+$ recipient mice, followed by LCMV clone 13 challenge. Two sets of adoptive-transfer experiments were performed; one using a low dose of donor cells (2,500 cells) and another with a large dose of donor cells (90,000 cells). The data shown in Fig. 3d, e are from the high-dose transfer experiment. Data in **b–d** are from the high-dose transfer; and in **e–h**

are from the low-dose transfer. **b**, Expansion of CXCR5^{+} CD8^{+} T cells in the blood after LCMV clone 13 infection. **c**, Number of cells in the spleen and liver 14 days after infection. **d**, Phenotypic analysis of transferred donor CXCR5^{+}Tim-3^{-} cells in the spleen 14 days after challenge showing proliferation and differentiation of this subset. Data are representative of 3 experiments (n=4 or 6 mice per experiment). **e**, Expansion of CXCR5^{+} CD8^{+} T cells (low dose transfer) in the blood after infection with LCMV clone 13. **f**, Number of cells in the spleen and liver 14 days after challenge. **g**, Phenotypic analysis of transferred donor CXCR5^{+}Tim-3^{-} and CXCR5^{-}Tim-3^{+} cells in the spleen and liver at 14 days after infection showing differentiation of CXCR5^{+} CD8^{+} T cells. **h**, Number of CXCR5^{+}Tim-3^{-} and CXCR5^{-}Tim-3^{+} CD8^{+} T cells derived from donor CXCR5^{+} or CXCR5^{-} CD8^{+} T cells in the spleen and liver after clone 13 challenge. Dashed line indicates the limit of detection. Data are combined from two experiments (n=8 or 10 per group, total n=18). Graph shows the mean and s.e.m. Student's t-test, where ** $P < 0.01$.

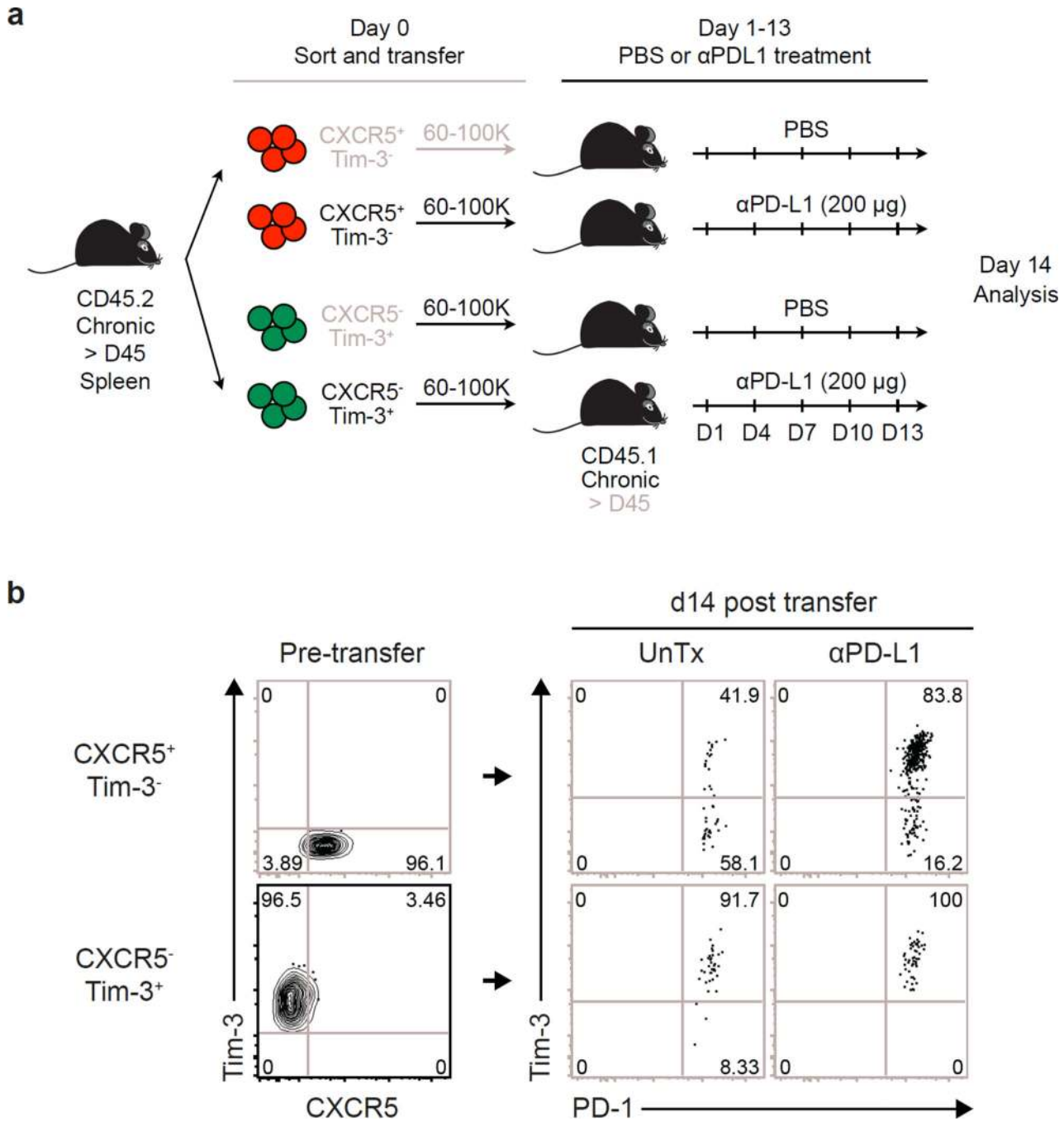

Extended Data Figure 10. Enhanced conversion of CXCR5$^+$Tim-3$^-$ CD8$^+$ T cells to Tim-3$^+$ CD8$^+$ T cells after PD-1 blockade

a, Sorted PD-1$^+$CXCR5$^+$Tim-3$^-$ and PD-1$^+$CXCR5$^-$Tim-3$^+$ CD8$^+$ T cells isolated from CD45.2$^+$ chronically infected mice (>45 days p.i.) were adoptively transferred into infection-matched CD45.1$^+$ recipient mice, followed by treatment with anti-PD-L1 antibody. **b**, Phenotypic analysis of sorted donor CD8$^+$ T cell subsets before transfer and 14 days after the transfer followed by PD-1 blockade. Data are representative of 2 experiments (total n=5, 7, or 9 mice per group).

Acknowledgments

R. Ahmed, A.H. Sharpe, and G.J. Freeman hold patents and receive patent royalties related to the PD-1 inhibitory pathway.

This work was supported by National Institutes of Health grants R01 AI30048 (R.A.), P01 AI056299 (R.A. and A.H.S.), R01 AI112579 (H.H.X.) and R01 AI121080 (H.H.X) and also by the Intramural Research Program of NIAID, NIH (R.N.G. and M.Y.G.). H.T.K. is supported by funding from the Prostate Cancer Foundation and Swim Across America. H.I.N. receives a CNPq research fellowship. The authors acknowledge technical support from R. Karaffa and S. Durham for cell sorting.

References

1. Zajac AJ, et al. Viral immune evasion due to persistence of activated T cells without effector function. J Exp Med. 1998; 188:2205–2213. [PubMed: 9858507]
2. Gallimore A, et al. Induction and exhaustion of lymphocytic choriomeningitis virus-specific cytotoxic T lymphocytes visualized using soluble tetrameric major histocompatibility complex class I-peptide complexes. J Exp Med. 1998; 187:1383–1393. [PubMed: 9565631]
3. Sharma P, Allison JP. The future of immune checkpoint therapy. Science. 2015; 348:56–61. [PubMed: 25838373]
4. Barber DL, et al. Restoring function in exhausted CD8 T cells during chronic viral infection. Nature. 2006; 439:682–687. [PubMed: 16382236]
5. Blackburn SD, Shin H, Freeman GJ, Wherry EJ. Selective expansion of a subset of exhausted CD8 T cells by alphaPD-L1 blockade. Proc Natl Acad Sci U S A. 2008; 105:15016–15021. [PubMed: 18809920]
6. Blackburn SD, et al. Coregulation of CD8+ T cell exhaustion by multiple inhibitory receptors during chronic viral infection. Nat Immunol. 2009; 10:29–37. [PubMed: 19043418]
7. Jin HT, et al. Cooperation of Tim-3 and PD-1 in CD8 T-cell exhaustion during chronic viral infection. Proc Natl Acad Sci U S A. 2010; 107:14733–14738. [PubMed: 20679213]
8. Paley MA, et al. Progenitor and terminal subsets of CD8+ T cells cooperate to contain chronic viral infection. Science. 2012; 338:1220–1225. [PubMed: 23197535]
9. Quigley MF, Gonzalez VD, Granath A, Andersson J, Sandberg JK. CXCR5+ CCR7− CD8 T cells are early effector memory cells that infiltrate tonsil B cell follicles. Eur J Immunol. 2007; 37:3352–3362. [PubMed: 18000950]
10. Kim HJ, Verbinnen B, Tang X, Lu L, Cantor H. Inhibition of follicular T-helper cells by CD8(+) regulatory T cells is essential for self tolerance. Nature. 2010; 467:328–332. [PubMed: 20844537]
11. Monney L, et al. Th1-specific cell surface protein Tim-3 regulates macrophage activation and severity of an autoimmune disease. Nature. 2002; 415:536–541. [PubMed: 11823861]
12. Matloubian M, Kolhekar SR, Somasundaram T, Ahmed R. Molecular determinants of macrophage tropism and viral persistence: importance of single amino acid changes in the polymerase and glycoprotein of lymphocytic choriomeningitis virus. J Virol. 1993; 67:7340–7349. [PubMed: 7693969]
13. Takeda K, Kaisho T, Akira S. Toll-like receptors. Annu Rev Immunol. 2003; 21:335–376. [PubMed: 12524386]
14. Crotty S. Follicular helper CD4 T cells (TFH). Annu Rev Immunol. 2011; 29:621–663. [PubMed: 21314428]
15. Yang CY, et al. The transcriptional regulators Id2 and Id3 control the formation of distinct memory CD8+ T cell subsets. Nat Immunol. 2011; 12:1221–1229. [PubMed: 22057289]
16. Pearce EL, et al. Enhancing CD8 T-cell memory by modulating fatty acid metabolism. Nature. 2009; 460:103–107. [PubMed: 19494812]
17. Cui G, et al. IL-7-Induced Glycerol Transport and TAG Synthesis Promotes Memory CD8+ T Cell Longevity. Cell. 2015; 161:750–761. [PubMed: 25957683]
18. Reya T, et al. A role for Wnt signalling in self-renewal of haematopoietic stem cells. Nature. 2003; 423:409–414. [PubMed: 12717450]

19. Gerner MY, Kastenmuller W, Ifrim I, Kabat J, Germain RN. Histo-cytometry: a method for highly multiplex quantitative tissue imaging analysis applied to dendritic cell subset microanatomy in lymph nodes. Immunity. 2012; 37:364–376. [PubMed: 22863836]
20. Jung YW, Rutishauser RL, Joshi NS, Haberman AM, Kaech SM. Differential localization of effector and memory CD8 T cell subsets in lymphoid organs during acute viral infection. J Immunol. 2010; 185:5315–5325. [PubMed: 20921525]
21. Mueller SN, et al. Viral targeting of fibroblastic reticular cells contributes to immunosuppression and persistence during chronic infection. Proc Natl Acad Sci U S A. 2007; 104:15430–15435. [PubMed: 17878315]
22. Anderson KG, et al. Intravascular staining for discrimination of vascular and tissue leukocytes. Nat Protoc. 2014; 9:209–222. [PubMed: 24385150]
23. Haynes NM, et al. Role of CXCR5 and CCR7 in follicular Th cell positioning and appearance of a programmed cell death gene-1high germinal center-associated subpopulation. J Immunol. 2007; 179:5099–5108. [PubMed: 17911595]
24. Shiow LR, et al. CD69 acts downstream of interferon-alpha/beta to inhibit S1P1 and lymphocyte egress from lymphoid organs. Nature. 2006; 440:540–544. [PubMed: 16525420]
25. Yamazaki C, et al. Critical roles of a dendritic cell subset expressing a chemokine receptor, XCR1. J Immunol. 2013; 190:6071–6082. [PubMed: 23670193]
26. Xu L, et al. The transcription factor TCF-1 initiates the differentiation of T(FH) cells during acute viral infection. Nat Immunol. 2015; 16:991–999. [PubMed: 26214740]
27. Choi YS, et al. LEF-1 and TCF-1 orchestrate T(FH) differentiation by regulating differentiation circuits upstream of the transcriptional repressor Bcl6. Nat Immunol. 2015; 16:980–990. [PubMed: 26214741]
28. Wu JQ, et al. Tcf7 is an important regulator of the switch of self-renewal and differentiation in a multipotential hematopoietic cell line. PLoS Genet. 2012; 8:e1002565. [PubMed: 22412390]

References for methods

29. Matloubian M, Concepcion RJ, Ahmed R. CD4+ T cells are required to sustain CD8+ cytotoxic T-cell responses during chronic viral infection. J Virol. 1994; 68:8056–8063. [PubMed: 7966595]
30. Wherry EJ, Blattman JN, Murali-Krishna K, van der Most R, Ahmed R. Viral persistence alters CD8 T-cell immunodominance and tissue distribution and results in distinct stages of functional impairment. J Virol. 2003; 77:4911–4927. [PubMed: 12663797]
31. Masopust D, et al. Dynamic T cell migration program provides resident memory within intestinal epithelium. J Exp Med. 2010; 207:553–564. [PubMed: 20156972]
32. Murali-Krishna K, et al. Counting antigen-specific CD8 T cells: a reevaluation of bystander activation during viral infection. Immunity. 1998; 8:177–187. [PubMed: 9491999]
33. Johnston RJ, et al. Bcl6 and Blimp-1 are reciprocal and antagonistic regulators of T follicular helper cell differentiation. Science. 2009; 325:1006–1010. [PubMed: 19608860]
34. Ivanova NB, et al. A stem cell molecular signature. Science. 2002; 298:601–604. [PubMed: 12228721]
35. Joshi NS, et al. Inflammation directs memory precursor and short-lived effector CD8(+) T cell fates via the graded expression of T-bet transcription factor. Immunity. 2007; 27:281–295. [PubMed: 17723218]
36. Miyazaki M, et al. The E-Id protein axis modulates the activities of the PI3K-AKT-mTORC1-Hif1a and c-myc/p19Arf pathways to suppress innate variant TFH cell development, thymocyte expansion, and lymphomagenesis. Genes Dev. 2015; 29:409–425. [PubMed: 25691468]
37. Allen CD, et al. Germinal center dark and light zone organization is mediated by CXCR4 and CXCR5. Nat Immunol. 2004; 5:943–952. [PubMed: 15300245]

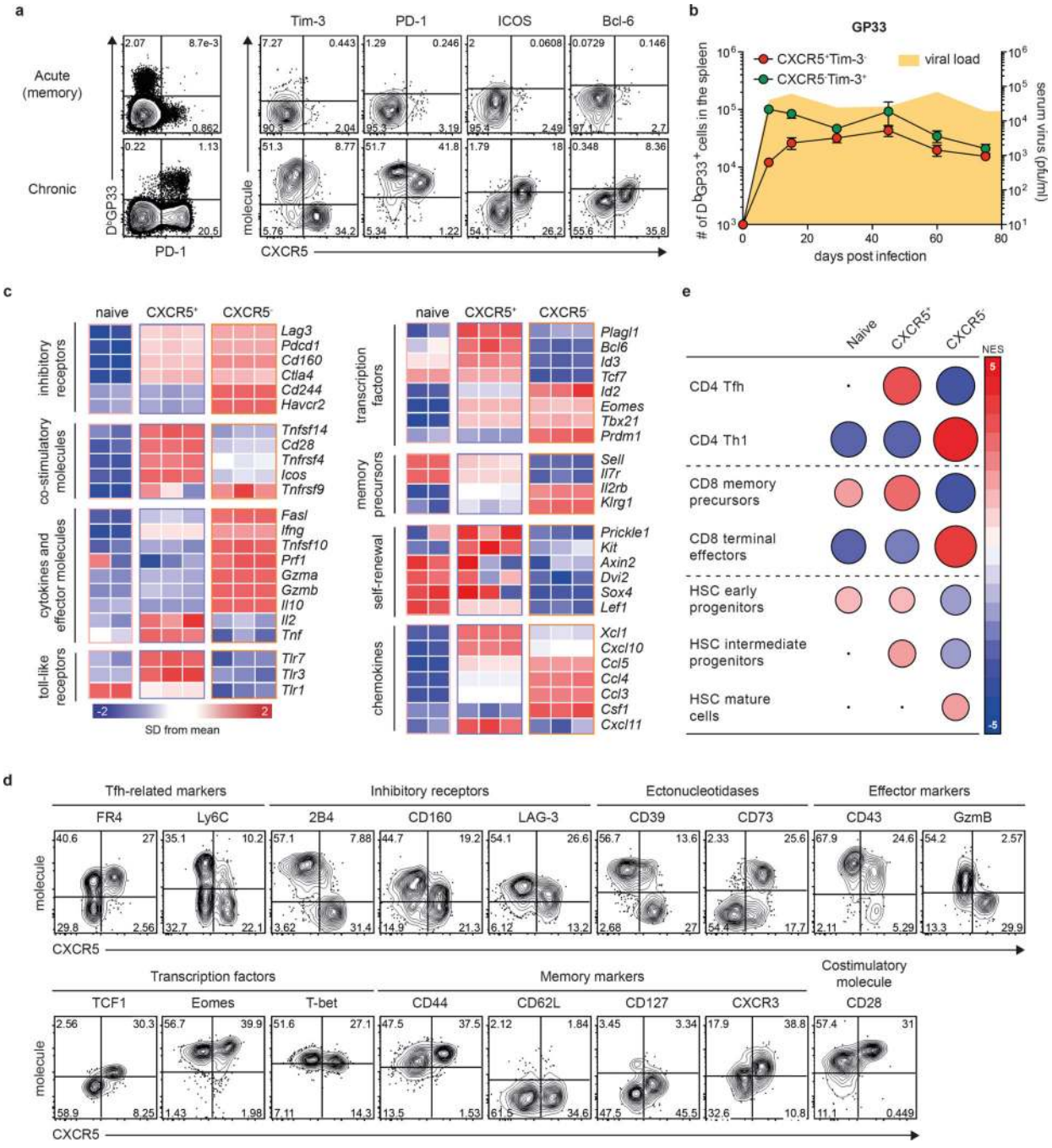

Figure. 1. Identification of a population of PD-1$^+$ CD8$^+$ T cells during chronic LCMV infection that has a unique gene signature that resembles both CD4$^+$ T$_{FH}$ cells and CD8$^+$ memory precursor T cells

a, Phenotypic analysis of GP33-specific CD8$^+$ T cells in the spleens of mice infected with LCMV Armstrong (acute) or clone 13 (chronic) at day 30 post infection (p.i.). **b**, Longitudinal analysis of the numbers of GP33-specific CXCR5$^+$ and CXCR5$^-$ CD8$^+$ T cells in the spleens of chronically infected mice (n=8 from two experiments per time point). Graph shows the mean and s.e.m.. **c**, Heat map illustrating the relative expression of genes in naïve CD8$^+$ T cells from uninfected mice and CXCR5$^+$Tim-3$^-$PD-1$^+$ and

CXCR5^{-}Tim-3^{+}PD-1^{+} CD8^{+} T cells from chronically infected mice (>45 days p.i.). **d**, Phenotypic characterization of CXCR5^{+} and CXCR5^{-} GP33-specific CD8^{+} T cells in the spleens of chronically infected mice (>45 days p.i.). **e**, GSEA for identifying specific gene signatures of the two CD8^{+} T cell subsets from chronically infected mice compared to gene signatures of different subsets of CD4^{+} and CD8^{+} T cells and haematopoietic stem cells. HSC, haematopoietic stem cell; NES, normalized enrichment score.

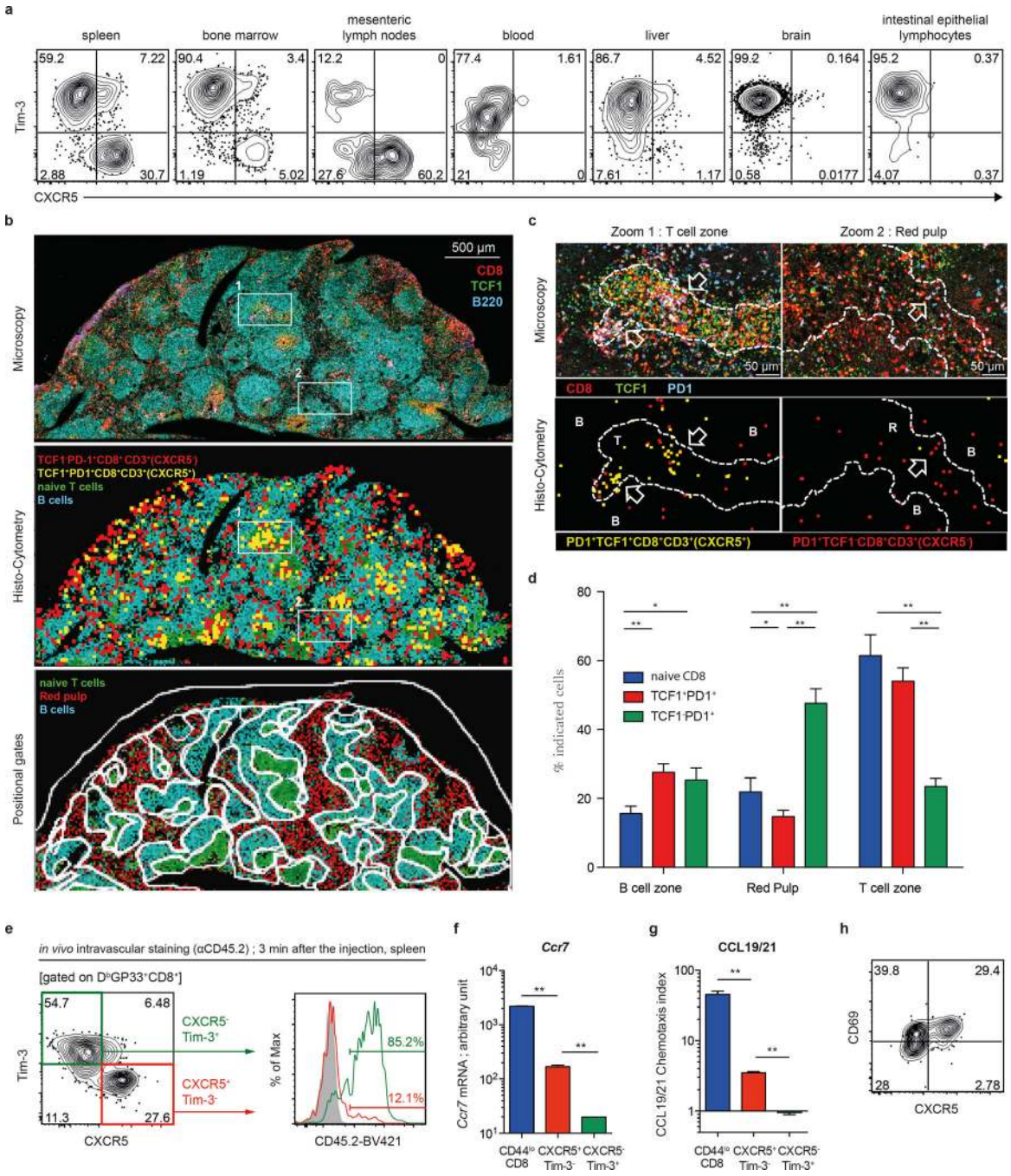

Figure 2. CXCR5$^+$ PD-1$^+$ CD8$^+$ T cells are found in lymphoid tissues of chronically infected mice and reside predominantly in T cell zones

a, Frequency of PD-1$^+$CXCR5$^+$Tim-3$^-$ and PD-1$^+$CXCR5$^-$Tim-3$^+$ LCMV-specific (GP33+GP276) CD8$^+$ T cells in the indicated tissues (45 days p.i.). **b**, Representative histology of the spleen and nuclear histocytometry analysis to identify the anatomic location of the two CD8$^+$ T cell subsets in chronically infected mice. **c**, Zoomed-in panels for the T cell zone and the red pulp. T, T-cell zone; R, red pulp; B, B-cell zone. **d**, Frequency of the CD8$^+$ T cell subsets within the respective zones. Data are representative of 3 experiments

(n=3 per experiment). **e**, *In vivo* CD45.2 labelling of CXCR5^{+} and CXCR5^{-} GP33-specific CD8^{+} T cells in spleen, 3 min after injection (n=4). **f**, Relative gene expression of *Ccr7* mRNA in sorted CD8^{+} T cell subsets. **g**, Migration of sorted CD8^{+} T cell subsets in response to CCL19 and CCL21. Data are combined from 2 experiments done in duplicate wells. **h**, CXCR5 and CD69 expression on GP33-specific CD8^{+} T cells. Graph shows the mean and s.e.m.. Student's t-test, where **P< 0.01; *P< 0.05. BM, bone marrow; mLN, mesenteric lymph nodes; IELs, intestinal epithelial lymphocytes; AU, arbitrary units.

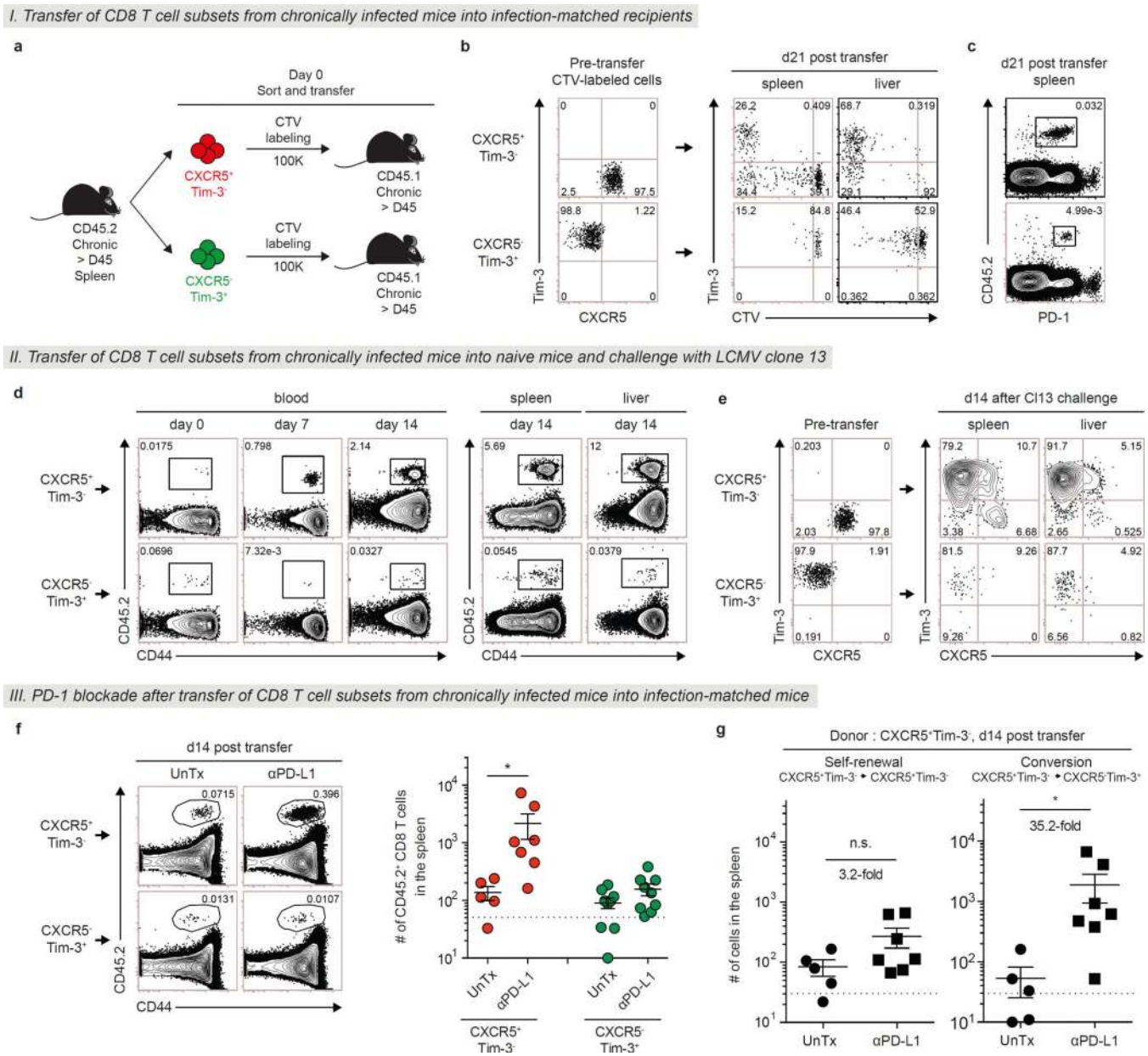

Figure 3. CXCR5$^+$ CD8$^+$ T cells act as stem cells during chronic LCMV infection and respond to PD-1 blockade

a, Experimental set-up showing transfer of congenically marked CTV-labelled PD-1$^+$CXCR5$^+$Tim-3$^-$ and PD-1$^+$CXCR5$^-$Tim-3$^+$ CD8$^+$ T cells from chronically infected mice into infection-matched recipient mice. **b**, Proliferation and differentiation of CXCR5$^+$ CD8$^+$ T cells in spleen and liver after adoptive transfer. **c**, FACS plots of donor CD8$^+$ T cells in the spleen. Data are representative of 3 experiments (total n=7 or 14 mice per group). **d**, Representative FACS plots showing expansion of donor CXCR5$^+$ CD8$^+$ T cells after transfer into naïve mice followed by LCMV clone 13 infection (see Extended Data Fig. 9a for experimental setup). **e**, Phenotypic analysis of donor CD8$^+$ T cell subsets pre-transfer and 14 days after transfer and clone 13 infection. Data are representative of 3 experiments (n=4 or 6

per experiment). **f**, FACS plots and total number of donor $CD8^+$ T cells recovered after adoptive transfer of $CXCR5^+$ and $CXCR5^-$ $CD8^+$ T cells into infection-matched recipient mice followed by PD-1 blockade (see Extended Data Fig. 10a for experimental setup) **g**, Expansion and differentiation of $CXCR5^+$ $CD8^+$ T cells after PD-1 blockade. Dashed line indicates the limit of detection. Data are combined results of 2 experiments and are mean ± s.e.m. Student's t-test, where $*P < 0.05$.

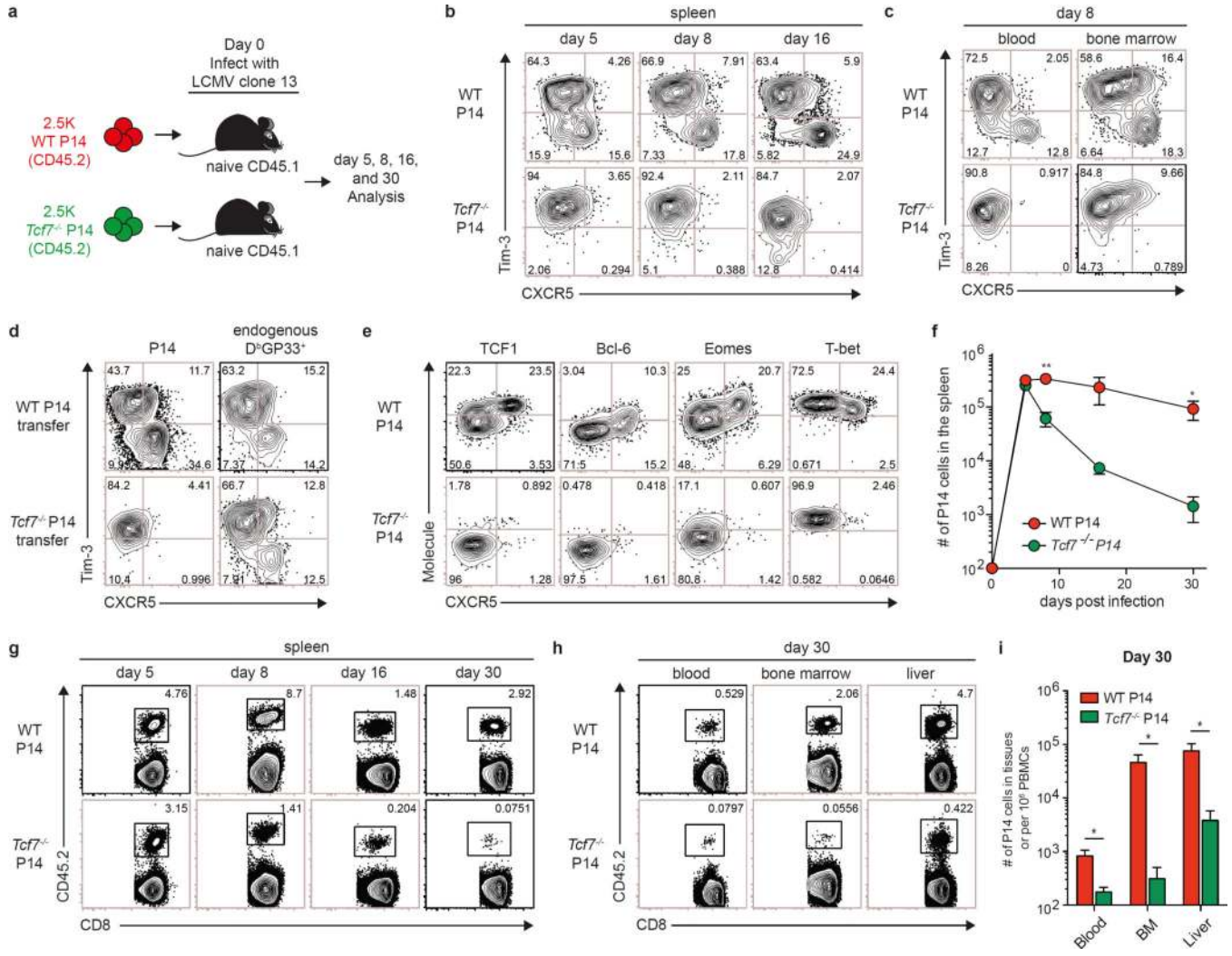

Figure 4. TCF1 is required for the generation of CXCR5$^+$ CD8$^+$ T cells during chronic LCMV infection

a, Congenically marked wild-type or *Tcf7*$^{-/-}$ LCMV GP33-specific P14 transgenic CD8$^+$ T cells were transferred into naïve mice, followed by LCMV clone 13 infection. **b,c,** CXCR5 and Tim-3 expression on wild-type and *Tcf7*$^{-/-}$ P14 cells in the spleen (b) and in tissues (c) at the indicated time points. **d**, CXCR5 and Tim-3 expression on wild-type or *Tcf7*$^{-/-}$ donor P14 cells and on endogenous GP33-specific CD8$^+$ T cells in the spleen 20 days p.i. **e**, Phenotypic analysis of wild-type and *Tcf7*$^{-/-}$ P14 cells in the spleen 8 days p.i. **f,g,** Longitudinal analysis of the numbers (f) and FACS plots (g) of wild-type and *Tcf7*$^{-/-}$ P14 cells in the spleen after clone 13 infection. **h,i,** FACS plots (h) and total number (i) of wild-type and *Tcf7*$^{-/-}$ P14 cells in the tissues 30 days p.i. Data are representative of 2 experiments (n=7 or 8 mice per time point). Graph shows the mean and s.e.m. Student's t-test, where **P < 0.01; *P < 0.05.